REPORT DOCUMENTATION PAGE

Form Approved
OMB No. 0704-0188

1. REPORT DATE *(DD-MM-YYYY)*	2. REPORT TYPE	3. DATES COVERED *(From - To)*
20-02-2013	Final	03/27/06 – 12/31/12

4. TITLE AND SUBTITLE
Corrosion Mechanisms in Brazed Al-Base Alloy Sandwich Structures as a Function of Braze Alloy & Process Variables. (Corrision Resistance of Superauthenitic Stainless Steel Sandwich Structures in Marines Environments Using Various Joining Technologies

5a. CONTRACT NUMBER
N/A

5b. GRANT NUMBER
N00014-06-1-0554

5c. PROGRAM ELEMENT NUMBER
N/A

6. AUTHOR(S)
J. R. Scully

5d. PROJECT NUMBER
N/A

5e. TASK NUMBER
N/A

5f. WORK UNIT NUMBER
N/A

7. PERFORMING ORGANIZATION NAME(S) AND ADDRESS(ES)

University of Virginia
Office of Sponsored Programs
P. O. Box 400195
Charlottesville, Virginia 22904-4195

8. PERFORMING ORGANIZATION REPORT NUMBER

125652-101-GG10825-31340

9. SPONSORING / MONITORING AGENCY NAME(S) AND ADDRESS(ES)
Office of Naval Research
875 North Randolph Street
Arlington, Virginia 22203-1995

10. SPONSOR/MONITOR'S ACRONYM(S)
N/A

11. SPONSOR/MONITOR'S REPORT NUMBER(S)
N/A

12. DISTRIBUTION / AVAILABILITY STATEMENT

Approved for public release, distribution unlimited.

13. SUPPLEMENTARY NOTES
N/A

14 AA 6061 (UNS A96061) and AA4047 (UNS A94047) were brazed to construct a tapered modelbraze joint with variable braze clearance. Isolated AA 6061 T6 was also exposed to the thermal cycle of a typical dip brazing process without applying filler metal. The braze, mixed, and heat affected zones were modeled by thermochemical computations and characterized experimentally. Corrosion exposures were conducted in accordance with BS 11846 Method B for detection of intergranular corrosion (IGC). Each zone developed its own corrosion morphology traced to the unique chemical composition and metallurgical characteristics. The brazing thermal cycle promoted IGC of isolated AA 6061. Moreover, the Al-Si braze and AA 6061 joint promoted additional intergranular corrosion in the Si containing mixed zone exacerbated by grain boundary Q ($Al_4Cu_2Mg_8Si_7$) and β phases as well as eutectically formed Sineedles at solidification boundaries. Pitting occurred in the Al-Si braze zone. Anodic and cathodic polarization scans were conducted on Al, Cu, Mg, heat treated AA 6061 sheet and selected synthesized intermetallic phases (Al_2Cu, Si, Mg_2Si, Al_2CuMg) in various NaCl solutions. These tests confirmed an unfavorable microgalvanic couple between grain boundary Mg_2Si and likely Q relative to both the Al-Cu-Mg alloy matrix and eutectically formed Si.

15. SUBJECT TERMS
dip brazing, intergranular corrosion, pitting corrosion, scanning electron microscopy, precipitation hardened aluminum

16. SECURITY CLASSIFICATION OF:			17. LIMITATION OF ABSTRACT	18. NUMBER OF PAGES	19a. NAME OF RESPONSIBLE PERSON
a. REPORT	b. ABSTRACT	c. THIS PAGE			J. R. Scully
Unclassified	Unclassified	Unclassified	UL	60	19b. TELEPHONE NUMBER *(include area code)* 434-982-5786

CORROSION MECHANISMS IN BRAZED AL-BASE ALLOY SANDWICH STRUCTURES AS A FUNCTION OF BRAZE ALLOY AND PROCESS VARIABLES:

Topic for Period of Performance
August 2009 to December 2012:

Metallurgical Factors Influencing the Aqueous Corrosion of Brazed Al-Mg-Si-(Cu) Alloy Joints Relevant to Cellular Metal Structures

John R. Scully, Ph.D.

Charles Henderson Professor of Materials Science and Engineering
Co-Director
Center for Electrochemical Science and Engineering
Department of Materials Science and Engineering
University of Virginia
School of Engineering and Applied Science
Charlottesville, VA 22904

Final Report UVA project number: GG 10825 125652

February 1, 2013

ONR Grant Number: N00014-06-1-0554

David A. Shifler, Ph.D., P.E.
Office of Naval Research, Suite 1425
875 N. Randolph Street
Code 332. Room 631
Arlington, VA 22203-1995
Phone: (703) 696-0285
Fax: (703) 696-0934
Email: david.shifler@navy.mil

1. Executive Summary

This project entails the study of the corrosion behavior of dip brazed AA 6061 and 4047; a low cost sandwich structure type joining process for use in possible land and sea applications. Brazed structures using both foil and paste as filler material were studied in both full immersion and accelerated laboratory testing.

This brazing cycle (T6TCT6) results in precipitation of Mg-Si rich β and Q particle and also the Al_2Cu θ phase to grain boundaries within the braze region. These phases and the Si-precipitated microstructure lead to a galvanic couple to the α-Al matrix and result in preferential dissolution of the braze region associated with intergranular corrosion likely promoted by Q phase precipitation. An alternate tempering cycle (T4TCT6) was studied in hope of reducing detrimental precipitation at the grain boundaries. However, significant precipitation and corrosion damage is seen within the braze region using the alternate tempering cycle.

These grain boundary precipitates were studied using TEM microscopy and EDS analysis. Grain boundary particles were rich in Mg and Si (β phase) and Mg, Si, Cu and Al (Q phase). Besides these 2 phases, the material also contained many constituent particles rich in Mg, Si, Cu, Fe and Cr. These precipitates promote inter granular corrosion within the braze region.

Additional investigations included the effect of minimizing the Cu content of the alloy and brazing material to reduce detrimental precipitate precipitation. Further TEM studies of grain boundary precipitation including characterization of the braze region confirmed presence of Q phase.

This final report is split into several technical sections after restating the technical objectives, needs and approach.

1. Corrosion of UNS A96061 Brazed with an Al-Si Alloy: Metallurgy and Corrosion Behavior. [section 5]
2. Temper Optimization of AA 6061 [section 6]
3. Mitigation by replacement of T4/barze/T6 temper with T4/braze/T6 temper and Mitigation by use of low Cu AA 6XXX alloys [section 7]
4. TEM Studies of Precipitates at Grain Boundaries in commercial AA 6061 T6 [section 8]
5. Projection Accomplishments [section 9]
6. Publications [section 10]
7. Human Resource Development [section 11]

Table of Contents

1. Executive Summary 2
2. Technical Objectives 5
3. Technological Needs and Scientific Questions 5
4. Technical Approach 6
PROPOSED OVERALL TECHNICAL OBJECTIVES 6
PROPOSED OVERALL APPROACH 7
5. Corrosion of UNS A96061 Brazed with an Al-Si Alloy: Metallurgy and Corrosion Behavior 8
ABSTRACT 8
EXPERIMENTAL PROCEDURE 12
Materials 12
Experimental and Modeling Procedures 13
Full Immersion Testing. 14
Transport and Metallurgy Modeling. 14
RESULTS 19
Brazed Joint Microstructures 19
Modeling of Brazed Joint: Braze, Mixed, and Thermally Cycled AA 6061 T6 Zones 20
Corrosion Analysis of Full Immersion Exposures of Brazed Joints 24
Corrosion Behavior of Thermally Cycled 6061 24
Corrosion Behavior of Brazed Joints 24
Electrochemical Analysis of Commercial AA 6061 after Aging 26
Electrochemical Analysis of Deconstructed Phases 26
DISCUSSION 27
Region 1: Pitting and Uniform Corrosion 27
Regions 2, 3, and 4: IGC and Pitting Corrosion 28
SUMMARY 29
ACKNOWLEDGEMENTS 30
REFERENCES 30
6. Temper Optimization of AA 6061 52
7. Mitigation by Reduced Cu content by using 6063T52 + AA4047 Filler Foil (Low Cu Variants) 53
8. TEM Studies of Precipitates at Grain Boundaries 54
9. Project Accomplishments 57

10. Publications 59
11. Human Resource Development (9 year history) 60

2. Technical Objectives

Corrosion is a major concern for any ultra-light cellular metal core sandwich panel exposed to salt water environments in both honeycomb and in open core structure and, in particular, at the nodes which attach facesheets and cores by brazing [14-20]. The impact of loss of facesheet/core bonding at nodes (a primary consequence of corrosion, but treated from the theoretical view as a severed bond in several papers) on structural properties has been investigated [21-22].

The objective of proposed braze research is establish corrosion mechanisms and modes in brazed Al precipitation age hardened alloys as a function of Al brazing alloys. Isolated brazed alloys as well as brazed joints at various diffusion lengths and variable Si and Cu levels are of interest. Therefore, the primary goal of this research is to establish to structure/composition/property paradigm at the microstructural length scale in braze, mixed zone and base material. The properties of interests are localized corrosion trends evaluated in exposures followed by characterization by microscopy and by electrochemical methods.

The closely related second objective is to explore thermal cycle and braze heat treatments-diffusion distance combinations that optimize melting point depressant diffusion into the base metal to produce the most optimal for corrosion resistance in brazed cellular metal joints exposed in marine environments. The combination of formation of a single homogeneous solid solution braze phase lacking corrosion prone intermetallics as well as a base metal lacking excess Si and/or coarse heterogeneously nucleated intermetallics offers the best strategy for intrinsic corrosion resistance in Al brazed alloys without the need for a diffusion barrier.

3. Technological Needs and Scientific Questions

There is the need to (a) understand the mechanisms of corrosion of brazed precipitation age hardened Al alloys exposed in marine alternate immersion and full immersion type environments, (b) propose mitigation strategies guided by the corrosion mechanisms established in (a) in order to extend the lifetimes and durability of brazed precipitation age hardened and other high strength Al alloys in marine environments. The challenge with transient liquid phase bonding, with respect to corrosion control in stainless steel or nickel base alloys, is to "match" or even overmatch the alloying composition that imparts excellent corrosion resistance to the braze structure equal to the base metal being brazed or remove melting point depressants such that excellent corrosion resistance can be maintained without sacrificing other desired braze properties such as joint strength and low melting point and wet ability. However, in the Al system, corrosion resistance is often optimized by either cladding with pure Al as a diffusion barrier, formation of Al-rich solid solution or by size and location control of intermetallic compounds (e.g., avoid grain boundary precipitation). If these are not possible then formation of

fine, homogeneously precipitated Si, Al-Cu, Al-Si or Al-Mg-Cu intermetallic phases is preferred over grain boundary phases that might trigger intergranular attack. Identification of the ideal braze alloy and processing conditions, from mechanical, metallurgical, and corrosion points of view needs to be the focus of research so that ultimately the beneficial properties of cellular metal structures can be preserved in harsh marine environments.

In order to advance the ability to develop joining technologies which optimize fabrication of cellular metal structures fabricated from brazed high strength Al, the following critical questions must be addressed in the case of brazed structures:

- What are the corrosion mechanisms and modes of attack of BAl-Si type commercial brazing alloys used with precipitation age hardened Al alloys both as isolated and combined phases? Does corrosion occur in the braze metal, intermixed zones or is it triggered in the base metal of brazed sandwich structures? What modifications in braze practice will extend the use of transient liquid phase bonded cellular metal structures to marine environments?
- Does excessive Si or other braze element diffusion into base material occur and is a diffusion barrier necessary to produce seawater corrosion resistant brazed Al 6061 structures?
- What composition and structures associated with commercially available braze alloys containing controlled alloying additions are predicted to optimize corrosion performance and be compatible with AA 6061 and 5052 from the standpoint of mitigating susceptibility to crevice, pitting and intergranular corrosion?
- Does any combination of initial braze time-temperatures or follow up heat treatment time-temperature-diffusion length (e.g., core-face sheet gap) combination enable formation of single phase, if any, solid solution braze microstructure or otherwise produce optimal corrosion resistance in Al? The preliminary literature review reveals that this is unlikely.
- What role if any do sandwich structures details and architecture play in influencing brazed Al panel corrosion resistance independent of microstructural details governed by alloy composition and microstructure scale phenomena.

4. Technical Approach

PROPOSED OVERALL TECHNICAL OBJECTIVES

The objective of proposed braze research is to establish corrosion mechanisms and modes in brazed Al precipitation age hardened alloys as a function of brazing alloys. Isolated brazed alloys as well as brazed joints at various diffusion lengths and this variable Si and Cu levels are of interest. Therefore, the primary goal of this research is to establish to structure/composition/property paradigm at the microstructural length scale in braze, mixed zone and base material. The properties of interest are localized corrosion trends evaluation by microscopy and electrochemical methods. The closely related second objective is to explore

thermal cycle and braze heat treatment combinations in isolated materials in relation to brazed cellular metal joints exposed in marine environments.

PROPOSED OVERALL APPROACH

Regarding brazing strategies to join Al-base sandwich structures, the brazing of one Al-base alloy with Al-Si with both a low and high Cu content. The experimental approach would involve study of isolated materials as well as a tapered brazed joint with variable clearance. Braze microstructure and composition will be characterized as a function of braze clearance (diffusion length) and processing parameters will be evaluated. The macro-electrochemical and microscopy probe techniques will be used to spatially assess corrosion performance which will be coupled with nanometer and micrometer scale characterization of braze, and braze-base metal intermixed zones. Corrosion resistance in each zone will be assessed and the microstructural/electrochemical basis for corrosion will be established. Moreover, unusual extrinsic mechanisms for attack of braze and basemetal will be assessed such as those caused by intermixing and wetting of base alloy grain boundaries, for instance, with excess Si, galvanically induced crevice and pitting corrosion as well as corrosion in eutectic braze microstructures. The minimum braze clearance for formation of a single phase braze microstructure if any is possible to form, will be identified.

These experimental studies will be augmented by equilibrium phase determination of braze alloy and base alloy microstructures as a function of variable Si, Mg, and Cu contents (e.g., melting point depressant) and temperature in Al-Si and Al-Si-Cu system. Either Thermocalc™ or FactSage™ software would be used in these determinations. Mechanistic information regarding governing factors will guide optimization of braze compositions and processing conditions. Secondary factors such as flux removal will not be pursued as these concerns are readily overcome by existing engineering best-practices.

5. Corrosion of UNS A96061 Brazed with an Al-Si Alloy: Metallurgy and Corrosion Behavior

Katherine M. Fleming, Aiwu Zhu, John R. Scully

Center for Electrochemical Science and Engineering, Department of Materials Science and Engineering

University of Virginia

395 McCormick Rd.

Charlottesville, VA 22904

ABSTRACT

AA 6061 (UNS A96061) and AA4047 (UNS A94047) were brazed to construct a tapered model braze joint with variable braze clearance. Isolated AA 6061 T6 was also exposed to the thermal cycle of a typical dip brazing process without applying filler metal. The braze, mixed, and heat affected zones were modeled by thermochemical computations and characterized experimentally. Corrosion exposures were conducted in accordance with BS 11846 Method B for detection of intergranular corrosion (IGC). Each zone developed its own corrosion morphology traced to the unique chemical composition and metallurgical characteristics. The brazing thermal cycle promoted IGC of isolated AA 6061. Moreover, the Al-Si braze and AA 6061 joint promoted additional intergranular corrosion in the Si containing mixed zone exacerbated by grain boundary Q ($Al_4Cu_2Mg_8Si_7$) and β phases as well as eutectically formed Si needles at solidification boundaries. Pitting occurred in the Al-Si braze zone. Anodic and cathodic polarization scans were conducted on Al, Cu, Mg, heat treated AA 6061 sheet and selected synthesized intermetallic phases (Al_2Cu, Si, Mg_2Si, Al_2CuMg) in various NaCl solutions. These tests confirmed an unfavorable microgalvanic couple between grain boundary Mg_2Si and likely Q relative to both the Al-Cu-Mg alloy matrix and eutectically formed Si.

Keywords: AA 6061/ UNS 96061, AA 4047/ UNS A94047, dip brazing, intergranular corrosion, pitting corrosion, scanning electron microscopy, precipitation hardened aluminum.

INTRODUCTION

Transient liquid bonding is a joining strategy that can accommodate intricate core designs involving aluminum alloy sandwich panels [1]. One class of heat treatable aluminum alloys used for sandwich structures are the 6xxx series of aluminum alloys. Alloys such as AA 6061 (97.52 wt% Al, 0.85 wt% Mg, 0.64 wt% Si, 0.22 wt% Cu, 0.48 wt% Fe, 0.1 wt% Mn, 0.18 wt% Cr, 0.04 wt% Zn, 0.06 wt% Ti, 0.02 wt% others) with a solidus temperature about 595^0C are readily brazed with Al-Si alloy filler materials [2]. Aluminum alloys selected as filler materials usually contain between 7 and 12 weight percent Si content incorporated as a melting point depressant. Alloys used in brazed AA 6061 [2] sandwich structures include AA 4145 (UNS A94145, Al-Si-Cu) and AA 4047 (UNS A94047, Al-Si), also referred to as types BAlSi-3 and BAlSi-4, respectively.

Consequently, the effect of elevated Si levels on IGC of AA 6061 (97.52 wt% Al, 0.85 wt% Mg, 0.64 wt% Si, 0.22 wt% Cu, 0.48 wt% Fe, 0.1 wt% Mn, 0.18 wt% Cr, 0.04 wt% Zn, 0.06 wt% Ti, 0.02 wt% others) is of great interest. The effect of Si and Cu on intergranular corrosion (IGC) of AA 6061 and related Al-Mg-Si alloys has been debated in the literature [3-7]. It is often reported that 6xxx series alloys that contain excess Si experience greater susceptibility to intergranular corrosion than balanced Al-Si-Mg alloys where all Si in consumed to form β–Mg_2Si [8]. Due to silicon's low solubility in aluminum [9], primary and eutectic Si forms when available in excess and becomes cathodic to the matrix creating a galvanic or localized corrosion cell. Si and Cu depletion in solute depleted zones, precipitation of Si and Cu containing phases, anodic dissolution of β–Mg_2Si along grain boundaries, and increased Cu contents have all been rationalized to cause IGC [6, 10]. However, in studies of 6xxx series aluminum alloys with excess Si, Cu was found to be more problematic than Si [6]. Hence, two distinct theories exist as to the initial causes of intergranular corrosion in 6XXX alloys. One theory links IGC to excess Si content while the other implicates Cu content in the alloy above 0.1 wt%. Less than 0.1 wt% copper helped mitigate intergranular corrosion Al-Mg-Si alloys with high Si contents [11]. European alloying practices favor excess Si (atomic fraction of Mg/Si < ~2) additions to improve strength. North American alloying

practices prefer to use a more balanced alloy that has Mg and Si contents in stoichiometric proportion, while adding up to 0.4 wt % Cu to achieve comparable strength. Cu additions are made to form coherent Q" and or Q' ($Al_4Cu_2Mg_8Si_7$) rather than θ' or θ" as the strengthening phase [12].

Thermal history is also an important factor during local corrosion of AA 6061. The time-temperature-composition combinations that produce pitting and intergranular corrosion on 6xxx series type alloys have been mapped [13]. Isothermal holds on alloys with compositions similar to AA 6061 revealed a transition from pitting to intergranular corrosion due to artificial aging. A region of limited localized corrosion existed between the pitting and intergranular corrosion regimes [13]. Larsen et al. [7] studied model Al-Mg-Si-Cu alloys with compositions similar to AA 6061. A nanoscale Cu rich film on grain boundaries of Cu containing variants of this alloy was believed to be a precursor to the formation of grain boundary Q phase ($Al_4Cu_2Mg_8Si_7$) [6]. This Cu film interacts with the surrounding solute depleted zones and matrix, especially in underaged conditions, to form local microgalvanic couples leading to IGC. Aging to T6 temper was argued to nearly eliminate IGC susceptibility in model alloys [14] by coarsening and breaking the continuous cathodic nanoscale Cu film. Overaging produced Mg depletion along grain boundaries as well as copious Q precipitate while coherent Q' precipitated in the matrix. I n the case of high Cu content, some alloys may show some susceptibility to intergranular corrosion that is associated with the formation of precipitate-free zones which are depleted of Cu and Si at grain boundaries and, as a consequence, are anodic with respect to the grains [13]. A series of recent papers on the corrosion of AlMgSi(Cu) alloys review these findings [8, 11, 14, 15].

Brazed materials often suffer from enhanced corrosion within the brazed region [16]. Brazing AA 6061 with BAlSi-2 (6.8-8.2 wt% Si, 0.25 wt% Cu, 0.2 wt% Zn, 0.1 wt% Mn, 0.8 wt% Fe), BAlSi-3 (9.3–10.7 wt% Si, 3.3-4.7 wt% Cu, 0.15 wt% Mg, 0.2 wt% Zn, 0.15 wt% Mn, 0.8 wt% Fe), and BAlSi-4 (11–13 wt% Si, 0.3 wt% Cu, 0.1 wt% Mg, 0.2 wt% Zn, 0.15 wt% Mn, 0.8 wt% Fe) introduces many of the compositional and microstructural effects discussed above as well as some additional concerns. These braze alloys use a high Si content to produce a low melting Al-Si near eutectic alloy. The recommended

brazing temperature for AA 6061 ranges from 582°C to slightly above 588° C with a solidus temperature near 582°C. Si is nearly insoluble in Al with a low solubility limit below 2% at the eutectic temperature [9]. Nearly 100 pct Al-Si eutectic phase is typically formed in the braze zone typical of near-eutectic compositions. Varying braze gaps are typically found in existing extruded tube and rolled sheet aluminum alloy cellular structures raise the question of how much Si depletion may occur [1, 17-19].

The corrosion of a base 6xxx series alloy increases in complexity when brazed especially considering the effects of Si and Cu on IGC. Brazed BAlSi-3 (AA 4145; Al, 11-13%Si, 0.3%Cu max, 0.8%Fe max, 0.15%Mn max, 0.2%Zn max wt%) joined with AA 6061 pitted and corroded intergranularly in 3.5% NaCl solution [20]. Polarization scans on AA 6061 T6 vacuum brazed with Al-12%Si braze filler in 3.5% NaCl aqueous solution aided interpretation [16]. Selective dissolution of the Al rich portion of the Al-Si eutectic occurred in the Al-9% Si filler metal after brazing because of the pitting potential of the Al rich region of the Al-Si eutectic phase was below the high OCP (open circuit potential) of Si [21]. Selective corrosion of the Al rich portion of the Al-Si eutectic microstructure was also reported by Kuroda [21]. In addition, large amounts of Cu added to the Al-Si filler material enhanced corrosion susceptibility [21]. However, the complex effects of Si on mixed braze and heat affected zones as well as the effects of braze gap on this phenomena have not been considered. The exact microstructures formed and the resultant mechanisms of IGC in brazed AA 6061 materials containing high levels of excess Si remains uncertain. Moreover, it is unclear (a) what affect the braze thermal cycle has on AA 6061, (b) what affect Si transported from the braze has on the metallurgy and corrosion of AA 6061, and (c) what affect a Si solidification structure has on the IGC of AA 6061 given the concerns for both Si and Cu in IGC.

The objective of this paper is to characterize the microstructure – corrosion relationship in each braze zone and deconstruct the phase/precipitate corrosion behavior of both the parent alloy and the braze fillers. Based on this information an attempt will be made to understand the mechanisms by which intergranular and pitting corrosion occur in brazed wedge coupons which simulate various braze gaps.

EXPERIMENTAL PROCEDURE

Materials

Two tempers of AA 6061 were used: 4.78 mm thick AA 6061 T6 and 4.83 mm thick AA 6061 T4 rolled sheets. AA 6061 T6 sheet at (4.78 mm and AA 4047 sheet at 76 μm thickness) were used to assemble dip brazed tapered wedges. Their respective chemical compositions are listed in Table 1.

Isolated samples included AA 6061 T4, AA 6061 T6, and an AA 6061 T6 sample heat treated to duplicate the thermal cycle a dip brazed cellular structure experiences during brazing and subsequent reaging to achieve the T6 temper a second time. Hereafter, this condition will be referred to as the TCT6 condition. The TCT4 sample consisted of an AA 6061 T6 sample heat treated to duplicate the thermal cycle that a dip brazed cellular structure experiences from followed by natural aging at room temperature. A few AA 6061 T6 samples were additionally solution heat treated at 540^{o}C for 1.5 hours, water quenched, and refrigerated; these samples are referred to as AA 6061 T6 SHTQ (AA 6061 T6 solution heat treat and quench). Due to the ability of AA 6061 T6 SHTQ to naturally age, all samples were tested within 2 days of heat treatment and were stored in a freezer prior to testing to minimize aging affects. SEM images were taken of these conditions after mechanically polishing and electropolishing in a chilled solution. Micrographs of these thermal conditions are seen in Figure 2. The precipitates are likely Q phase and/or β phase (Mg_2Si) [22].

High purity Mg (99.9%) rod and undoped single crystal 100% Si wafers were also tested. Additionally, some phases and precipitates were cast: Al_2Cu and Mg_2Si. 99.99% pure Cu ingot and 99.99% pure Al sheet were used to induction melt Al_2Cu (θ phase) in an argon (Ar) gas environment. Al_2CuMg samples were fabricated externally.[1] For Mg_2Si (β phase) synthesis, 99.99% purity Mg and

[1] Synthesis of the S phase intermetallic was performed at both Alcoa and Sandia National Laboratory. Al_2CuMg samples (S phase) contained Al_2CuMg + AlCuMg+ α- Al. Both S-phase alloys exhibited similar electrochemical behavior. Only the Alcoa produced S phase is included here for simplicity.

undoped pure Si wafer were melted in a crucible at Monash University[2]. $Al_4Cu_2Mg_8Si_7$ (Q phase) was not available.

Tapered wedge samples were constructed using AA 6061 T6 plates of 4.78 mm thickness and had a variable tapered braze gap ranging from 80 to 200 μm. Wedges were 2.5 cm in width by 12.5 cm in length. The wedge gap was filled by dip brazing AA 6061 T6 with AA 4047 (BAlSi-4) filler foil. A typical dip brazing process was performed with temperatures as seen in Figure 1 [23]. Cleaning treatments were performed at temperatures well below 100^0C. Assembled, foil filled and clamped wedges were placed in a preheat furnace at 538^0C for 15 minutes at 1 atm in air. In actual brazed sandwich structures this time would be dictated by cellular structure size. Upon reaching 538^0C, the structure was then moved from the preheat furnace to the flux bath and dipped.[3] These wedges were dipped for 15 to 30 seconds in hot flux no more than twice. After full immersion in the flux bath, the part was fan cooled to room temperature with cooling rates from 0.08 K/s up to 0.32 K/s at the fastest cool. Again, low temperature cleaning treatments were performed. Then the wedge was aged at room temperature for 4 days to T4 temper. After achieving T4 temper, the part was placed into a furnace and aged for 18 hours at 163^0C to precipitation harden and achieve a T6 temper. Upon completion of wedge construction the wedges were cross-sectioned every 1 cm along the length to study various braze gap thicknesses.

Experimental and Modeling Procedures

Microstructures as a function of position from the braze zone and gap were imaged with submicrometer resolution on electropolished surfaces using field emission gun scanning electron microscopy (JEOL 6700F) at either 10 kV or 15 kV and 10 μA. A working distance of 15 mm and an accelerating voltage of three times the energy of the maximum characteristic peak of interest were used for EDS. Secondary electron imaging in LEI mode was found to identify topography as well as phases.

---

[2] Monash University is thanked for synthesis of the β phase intermetallic.

[3] This dipping process is dependent on part size and thickness and typically ranges from 15 seconds to 1 minute. A part may be dipped in hot flux up to three times in this process, but typically will not exceed two dips.

Preparation for SEM included grinding with SiC paper in water to 1200 grit and then polishing with 1 μm diamond paste. Samples were then sonicated in deionized water for 5 minutes and dried. Electropolishing was conducted between -32 to -37°C under a liquid nitrogen chill at 11.2 V for one minute [10]. The electropolishing solution was a mixture of 1/3 concentrated Nitric acid (HNO_3) and 2/3 Methanol (CH_3OH) by volume. Post electropolishing, samples were rinsed with deionized water and dried immediately. Vickers micro hardness marker indentations of 200 g for 20 s were used for site recognition and post corrosion test evaluation. Samples were imaged both before and after full immersion testing.

Full Immersion Testing.

Exposures were adapted from BS 11846 Method B [24]. The BS 11846 Method type B is reported to produce results on precipitation hardened Al alloys which provide a good indicator of long term field exposure performance in natural environments [15]. BS 11846 Method B was performed initially and found to be highly corrosive over a 24 hours period. In order to understand the corrosion mechanisms at the microstructural length scale, especially those related to phases, shorter times of 2, 4, 6,8 and 10 hours were tested and imaged; ultimately 8 hours of full immersion in BS 11846 Method B acidified salt solution (0.51 M NaCl + 12 mL 10.0 N concentrated HCl per liter, pH=1.2, ambient temperature aeration) was selected as the optimum time to observe corrosion. After SEM imaging was completed, samples were repolished approximately 5 μm with 1 μm diamond paste to remove the effects of electropolishing and were exposed under full immersion in BS 11846 Method B ambient temperature aeration solution for 8 hours. A concentrated Nitric acid (HNO_3) dip for 15 seconds removed corrosion products prior to post-exposure SEM imaging [25].

Transport and Metallurgy Modeling.

In order to first understand microstructures in the brazed, mixed, and AA 6061 zones and help predict potential detrimental phases that may trigger pitting and intergranular corrosion, models were

developed to simulate elemental transport during brazing, as well as phase diagrams, equilibrium phase fraction diagrams[4], continuous cooling curves, and time temperature transformation curves for a series of Al, Al-Mg-Si, and Al-Mg-Si-Cu alloys. A 100 μm AA 4047 (BAlSi-4) filler foil with a planar interface with AA 6061 was modeled with a cooling rate of 0.08 K/s. The compositions listed in Table 4 were used for modeling purposes.

Calculations of chemical concentration profiles perpendicular to the initial interface of the base plate and the filler material were based on one dimensional atomic diffusion [26] and were primarily dependent on heating and cooling rates. The duration the assembled cellular sandwich panels dwell in the flux bath is short in comparison to the heating and cooling times, and it was assumed to be 30 seconds per dip in molten flux based on input from the manufacturer. The simulations for dipping the part in flux were calculated at typical brazing temperatures between 247 °C and 597 °C. It was assumed that second phases dissolve at temperatures higher than 527 °C. An Al FCC solid solution would not be liquid over most times in this scenario. The only temperatures where the liquid phase was assumed to exist were temperatures above the solvus, and also at temperatures 10 to 15 degrees below the solvus due to supercooling. Phase boundary mobility between FCC Al and liquid was neglected and Cu was assumed to have an insignificant impact on Si and Mg diffusion. All filler foil thicknesses were assumed to be 100 μm in width and all cooling rates were 0.08 K/s. Base plate thickness for all calculations was assumed to be much greater than 100 μm. Since diffusion occurs most efficiently at high temperatures around the melting point, the simulation of the dipping process was considered at temperatures above (247°C) 520 K and with a peak temperature of 870 K (497°C). Diffusion in the FCC solid solutions were modeled using assessed experimental data in publications and mobility parameters [27, 28]. For simplicity, the concentration dependence of diffusivity was neglected. The unknown Si-related off-diagonal diffusion coefficients were set to zero.

[4] Phase fractions are obtained by taking the number of atoms in a particular phase of interest relative to the total number of atoms present in all the phases of the alloy.

The CALPHAD (Calculation of Phase Diagrams and Thermochemistry) approach was used to predict equilibrium phase fractions. Chemical potential inputs were used in conjunction with published literature and existing databases [29, 30]. These calculations were performed for alloy concentrations. For all CCT (continuous cooling transformation) and TTT (time temperature transformation) curves, four secondary phases were assumed in most calculations: θ (Al_2Cu), Q ($Al_4Cu_2Mg_8Si_7$), β (Mg_2Si), and Si (diamond) as predicted by Laughlin [22]. S (Al_2CuMg) and T (Al_2MgSi) phases were not considered in the modeling for simplicity because they exist at very low temperatures and Si contents which are not relevant to the brazing processes described here. No phase separation was accounted for and all secondary phases precipitate from an Al FCC solid solution.

Homogeneous nucleation with and without preexisting nuclei as well as heterogeneous nucleation were considered for all calculations using a precipitation model [31]. Johnson-Mehl-Avrami kinetics were used [32]. In Al-Mg-Si alloys, the GP→β"→β' → β and QP→Q"→Q'→Q sequences describes the precipitation process [22]. Since the focus was on equilibrium phases formed at grain boundary, equilibrium β and Q were considered.[5] The crystalline parameters of the equilibrium form of these phases listed in Table 2 were used [30, 33-35]. The assumed compositions are given in Table 3 and other parameters are given in Table 4 for 6061 + Si alloys. It was assumed that the precipitation process of Q and β are controlled by slow mobility of Mg atoms [27]. Al_2Cu (θ) and Si phase formation was controlled by Cu and Si diffusion. For additional modeling parameters recent literature provided guidance [31].

Precipitation can also occur when embryos of second phases on local structural heterogeneities. Similar to preexisting atomic clusters and dislocations, grain-boundaries (GB) can be preferential nucleation sites for second phases for lower strain energy, higher solute diffusivity and possibly lower interfacial energy associated with their formation [36]. The overall energy change on forming a nucleus on GB may be written:

[5] In the case of the Beta phase, the crystal structure, lattice parameter, shape and orientation differ between metastable and equilibrium structures but not the composition. In the case of the Q phase, both metastable Q' and Q equilibrium compositions and structure are quite similar.

$$G_{total}=\Delta G_{\Phi}+\Delta G_{\gamma}+\Delta G_{\varepsilon}+\Delta G_{GB} \quad (1)$$

where ΔG_{γ} is the interfacial energy and ΔG_{ε} is the strain energy. Both were neglected in the calculation of homogeneous precipitation or assumed insignificant as compared with the chemical driving forces ΔG_{Φ}. The reduction in strain energy was attributed to destruction of that part of the elastic energy of GB that lies within the volume of the nucleus [36]. The strain energy reduction ($-\Delta G_{GB}$) due to the interaction between GBs and the second phase nuclei were estimated to be close to the value of the strain energy ΔG_{ε}, similar to precipitation at dislocations [37]. The strain energy was estimated using the elastic constants of the aluminum matrix and the 2nd phases and the misfit strain that was set as 0.05, as shown in Table 4. The site density for heterogeneous nucleation depends on d/D, where d is the thickness of grain boundaries and D grain size or average diameter of grains. The value of d was estimated to be 0.4 nm and D of100 μm was used. These assumptions were made for other parameters; the activation energy of GB diffusion is 2/3 of the corresponding values inside grains, and the interfacial energy ΔG_{γ} of grain boundary nuclei was reduced by 10% from that inside the grains.

The activation energy associated with grain boundary diffusion and the interfacial energy affected the TTT and CCT curves associated with GB precipitation of Q and β in the higher-Si (2.6 wt%) solid solutions. Considering continuous cooling, the temperature decreases through a series of discrete values $\{T_1, T_2, \ldots T_n\}$. The volume fraction f_i of a phase generated during one of those isothermal processes at temperature T_i for a period of time t_i can be written as:

$$f_i = t_i^4 / \beta_i(T_i)^4 \quad (2)$$

where $\beta_i(T_i)$ is a function of temperature representing effects of the diffusion, activation energies of nucleation and growth, and interfacial energies of the phase [31]. The total volume fraction generated during the whole cooling process is:

$$f = \sum_{1}^{n} f_i = \sum_{1}^{n} [\frac{t_{CCT}}{n\beta_i(T)}]^4 \quad (3)$$

For the isothermal process at T_i to generate f amount of the phase, where n is 0.25 and the summation n is the step at each incremental temperature. The total time, t_{CCT}, to generate a given volume fraction of a phase can be therefore written as:

$$t_{CCT} = \frac{n}{(\sum_{n} t_{TTT}^{-4})^{1/4}} \quad (4)$$

Using this formula, the extent of transformation as a function of time for a continuously decreasing temperature can be obtained. For TTT predictions, the time t for formation of the phase Φ with a minimal phase fraction f_v (0.5%) was estimated using:

$$t = \frac{\propto a_0^2 f_v^{1/4}}{D_{M,FCC}} \sqrt[4]{\frac{e^{G_\Phi^*/R_G T}}{(1-e^{G_\Phi/R_G T})^3}} = \beta(T) f^{1/4} \quad (5)$$

Where R_g is the molar gas constant, α_Φ is the structural constant set to1.0, a_0 is the atomic spacing, assumed to be 0.286 nm, $D_{M,FCC}$ is the effective diffusivity of solute atoms associated with both nucleation and early growth in the supersaturated FCC solutions, ΔG_Φ = chemical driving force (determined from CALPHAD), and G^*_Φ=the nucleation activation energy. G^*_Φ was calculated by the equation:

$$G_\Phi^* = \frac{K\gamma_\Phi^3 V_\Phi^2}{\Delta G_\Phi^2} \quad (6)$$

where V_Φ is the atomic volume (per atom), γ_Φ is the interfacial energy of the crystal phase Φ which is unknown, K is the shape factor (16π/3), ΔG_Φ^2 is the chemical driving force (from CALPHAD). Turnbull's equation [38] was used to estimate the interfacial energy of Φ:

$$\gamma_{\Phi} = 0.40 \times \frac{\Delta H_{f,\Phi}}{N^{1/3} V_{\Phi}^{2/3}} \quad (7)$$

where N is Avogadro's number, $\Delta H_{f,\Phi}$ is the formation enthalpy from FCC solid solution (CALPHAD), and V_{Φ} *is the* atomic volume (per atom).

Open Circuit (OCP) and Anodic Polarization Scans.

Aerated, anodic potentiodynamic scans were conducted on the commercial aluminum alloys and on synthesized metallurgical phases. Cathodic potentiodynamic scans were conducted on Si, Cu, and Al_2Cu. Tests were conducted at 25 ^{o}C under ambient aeration at 1 mV/sec after 30 min at OCP. The potentiodynamic tests were conducted in aerated 0.6 M NaCl solution and the BS 11846 Method B solution (0.51 M NaCl + 12 mL 10.0 N HCl per liter of solution; pH=1.2). Samples were ground to 1200-grit SiC paper, sonicated, and rinsed in acetone. Synthesized intermetallic phases were polished in the same manner, except for Mg_2Si which was ground in ethylene glycol up to 1200 grit and rinsed with acetone.

RESULTS

Brazed Joint Microstructures

The thermal process a cellular sandwich structure experiences during dip brazing is summarized in Figure 1. Figure 1 also shows the initial solution heat treatment, quench and precipitation heat treatment including quench recommended for AA 6061 extruded tube in a T6 temper as defined by ASTM [39]. The AA 6061 T6 condition resulted in grain boundary and matrix precipitation (Figure 2(a)). However, (Figure 2(b)) the AA 6061 T6 condition had less grain boundary precipitation and smaller overall grain boundary precipitates than the TCT6 condition. The thermal profile of the braze cycle

enhanced both grain boundary precipitate density and size as evident from comparison of Figures 2a and 2b.

Figure 3 shows the wedge design which simulates a brazed joint and includes the gap variations exaggerating what is found in an actual cellular sandwich panel. The tapered braze gap in an AA 6061 T6 + AA 4047 (BAlSi-4) foil wedge reheat treated to T6 temper after brazing was examined (Figure 4). The wedge gap varied between 80 – 200 μm. Three distinct zones were present regardless of gap: a braze zone, a resolidified "mixed zone," and an AA 6061 TCT6 zone as seen in Figure 3(b). For reference, the original AA 4047 (BAlSi-4) filler foil thickness was 76 μm as indicated by the dotted line in Figure 4, which shows a wedge sample after electropolishing. Nearly 100% Al-Si eutectic can again be seen where the original braze filler was located. The eutectic extends beyond the original foil thickness and represents mixing of Al-Mg-Si-Cu with Si. Resolidified AA 6061 formed coarse grains with Al-Si eutectic at solidification boundaries. This occurs as far away as 125 μm from the original interface of the AA 6061 T6 and the BAlSi-4 filler foil. AA 6061 was likely melted near the braze when additional Si content depressed the melting point of the Al-Mg-Si alloy. Therefore, the mixed zone consisted of liquated and resolidified AA 6061 in the form of coarse grains, precipitated Si, as well as Al-Si eutectic on solidification boundaries. The AA 6061 T6 beyond the region of Si transport has the original composition but experienced the thermal cycle in Figure 1 as evident from EDS analysis. EDS could not successfully define the composition of the white grain boundary precipitates seen in the AA 6061 T6 region of the wedge due to the large interaction volume for 15 kV incident electrons. This energy produced an Al interaction volume of 1.034 μm^3 which includes the underlying matrix.

Modeling of Brazed Joint: Braze, Mixed, and Thermally Cycled AA 6061 T6 Zones

Figure 5(a) shows the effect of 3 thermal cycles from dips in flux on the predicted Si concentration profiles perpendicular to the braze/6061 interface, with each successive dip enhancing the

high temperature Si enrichment outside of the braze gap and decreasing the Si content within the braze gap.[6] Similarly, Figure 5(b) shows the effect of 3 dips in flux on Mg content, with each successive dip decreasing the Mg content adjacent to the braze gap and enhancing the Mg content within the braze gap. Figure 5(c) displays the Si content as a function of each successive dip in flux at positions of 1, 20, and 100 μm, respectively, from the initial interface of AA 6061 T6 and the AA 4047 (BAlSi-4) foil. Finally, Figure 5(d) shows the concentration of Mg at 1, 20 and 100 μm from the interface. There is an increase with each dip in flux at 1 μm from the interface. These trends were always seen with only slight quantitative variations at different gaps and cooling rates.

Resulting compositions were used to predict the phases expected at equilibrium as a function of temperature in each zone. It is recognized that metastable phases instead of equilibrium phases may exist in reality. Nevertheless equilibrium phases should be considered as a reference point for grain boundaries after high temperature brazing. Recent literature [22] has discussed the phase transition in terms of the tetrahedron of phase fields [22]. Increasing the Mg, Cu, and Si contents is known to shift aluminum alloys between the 2xxx and 6xxx series and have a strong effect on the equilibrium and metastable phases that form. 6xxx series alloys form the strengthening β phase through a series of metastable phases [22]. With the addition of Cu, these 6xxx series alloys additionally form the quaternary Q phase ($Al_4Cu_2Mg_8Si_7$) [22]. When Si is added to the Al–Cu–Mg alloys, the three-phase field consisting of (Al), θ and S expands into the tetrahedron consisting of (Al), θ, S and β phases at low Si [22]. At higher Si, a cross over occurs to the tetrahedron in which Q replaces S, and the tetrahedron consists of the phases (Al),θ, β and Q, similar to those present when Cu is added to 6xxx alloys [22]. These phases were considered.

Figure 6 shows the predicted pseudo binary phase diagrams applicable for AA 6061 and AA 4047 (BAlSi-4) before brazing and the mixed zone after brazing consisting of Al-Mg-Si-Cu + excess Si. For

[6] The Si concentration profile is shown in Figure 5 for the high temperatures over which transport calculations were made. Once cooling occurs Si has low solubility in fcc Al. It is recognized that Si cannot exist in solid solution in Al and would either form eutectic Si or precipitates silicon in equilibrium with an Al rich solid solution.

reference, the brazing temperature is 593°C (876 K). The vertical dotted line shows the overall composition for expected pre and post braze materials in the indicated zones. Figure 6a indicates that the Al-Si euctectic transformation occurs just below 577 °C (850 K) at all Si levels above about 1.5%. Figure 6b shows that with increasing Si content, as seen in the mixed zone, Si acts as a melting point depressant lowering the melting temperature over a range of AA 6061 + Si compositions to as low as around 567 °C (840 K). This would enable a liquid phase to form in an Al-Mg-Si alloy. This melted portion of the structural AA 6061 material would thin reject Si into the liquid phase which eventually solidifies at the eutectic composition forming an Al-Si eutectic at the grain boundaries of the solidification microstructure. Nnew phases are possible at low temperatures and low Si contents by precipitation reactions– specifically θ (Al_2Cu), Q, β (Mg_2Si) phases and diamond cubic Si (Figure 6(c)). However, once Si is reduced below about 0.7%, neither eutectic Si or precipitated Si is expected.

Figure 7 shows the equilibrium phase fractions formed at infinite times at compositions representative of the braze, mixed and base plate zones. Figure 6 predicted the possible presence of Mg_2Si (β), Al_2Cu (θ), Q ($Al_4Cu_2Mg_8Si_7$), Si (diamond), in addition to a balance of FCC Al depending on composition. However, Al_2Cu (θ) is not seen in Figure 7 likely due to the assumption of the formation of Q at higher Si contents. Moreover, there is a shift from Al_2Cu (θ) to Mg_2Si (β) once Mg is introduced between the braze and mixed zones even at depleted levels relative to AA 6061. Figure 8 provides the predicted equilibrium phase fractions formed at infinite times as a function of compositions representative of the AA 6061 zones which have gained silicon from the braze foil. Mg_2Si (β) and Q ($Al_4Cu_2Mg_8Si_7$) are expected with Q the dominant phase at lower temperatures. As Si content drops, the Si phase and β phase are predicted to be possible while the Q phase is possible at a Si threshold of around 1 wt% Si (e.g., Figures 8(a) compared to 8(d). Precipitated Si decreases with the overall Si content and is no longer expected at 0.5% Si. Mg_2Si, Al_2CuMg and Al_2Cu are dominant phases instead of Q when the Si falls to 0.5% and Mg is maintained at 1%.

Recognizing the need to consider kinetics of phases formation, precipitation during both continuous cooling (CCT) (to model the continuous cooling after dipping in a flux bath) and time temperature transformation (TTT) to model the post braze heat treatment (18 hours at 163°C to achieve theT6 condition) were modeled. Figure 9 contains the simulations for regions 1 (braze zone) and 2. Figure 10a and b shows the CCT and TTT curves for Region 3. Figure 10c and d report the thermally cycled, but compositionally unaltered AA 6061 T6 in Region 4. All CCT curves in Figures 9-11 have three cooling rates indicated: 1 K/min, 10 K/min, and 30 K/min which bound typical cooling rates utilized (between 1 and 10 K/min). All TTT curves show the transformation times required to form 0.5% volume fraction of the phase considered. β-Mg_2Si is formed upon cooling and isothermal aging at all compositions. Q forms mainly upon isothermal aging or during the slowest cooling. Si is formed at 6% Si content. Silicon is not formed at 2.6% Si or below and is absent from the AA 6601 composition. Overall, increasing Si content shifts the nose of the TTT curve to shorter times for Si formation. Figure 11 compares homogeneous to heterogeneous nucleation at clusters and grain boundaries for the nominal AA 6061 composition + 2.6 wt% Si. Q and β formed so easily on grain boundaries compared to on clusters or by homogenous nucleation that they are expected upon cooling from the dip braze. This can be seen in Figure 11 at the AA 6061 composition with excess Si (2.6 wt% Si) for) for a reduced interfacial energy and diffusion energy at grain boundaries which are assumed to be 9/10 (IFE) and 2/3 (H) of those inside grains, respectively. Similar behavior is expected for the AA 6061 composition, but it is omitted here for brevity. CCT curves are reported, but TTT curves (not shown) have also been modeled and show similar trends. These grain boundary precipitates are seen in SEM micrographs (Figure 2 and Figure 4) and in published literature [6, 7, 22].

Figure 12a summarizes regions by distance from the initial interface and composition profile of the AA 4047 and AA 6061 T6 joint after brazing. Region 1 has the compositions of the AA 4047 filler foil (BAlSi-4). Region 2 spans from 1 μm to 19 μm from the original, unbrazed interface of the AA 4047 (BAlSi-4) filler foil and AA 6061 T6. Region 3 is from 20 to 99 μm relative to the initial interface.

Region 4 includes >100 μm from the initial interface, or 100 μm until the composition is that of AA 6061 T6. Figure 12b shows the electropolished microstructure with each zone labeled. Table 5 provides a summary of Regions (1, 2, 3 and 4), compositions, and the equilibrium phases expected to form and pertinent to the grain boundaries as a result of all the thermal processes experienced during dip brazing based on both the thermodynamic and homogeneous kinetic modeling. In Region 1, an Al-Si eutectic was formed and β and Q are possible precipitates formed upon aging after brazing. In Region 2, Si, β, and Q are likely to form. Region 3 is similar to Region 2 for phase formation except that Si is not likely to form. Region 4 has β and Q as likely phases formed. Region 4 behaves similar to AA 6061 but with the possible addition of S and θ phases commonly found in lower Si aluminum alloys with Mg and Cu [22] (Figure 8).

Corrosion Analysis of Full Immersion Exposures of Brazed Joints

Corrosion Behavior of Thermally Cycled 6061

Eight hour immersion testing in the acidified salt water solution per BS 11846 Method B revealed intergranular corrosion on AA 6061 as seen in Figure 13a-b. The AA 6061 T6 condition exhibits intergranular corrosion along grain boundaries (Figure 13a). The isolated TCT6 condition of AA 6061 also exhibits intergranular corrosion except that TCT6 condition shows more enhanced attack of the matrix (Figure 13b).

Corrosion Behavior of Brazed Joints

A wedge was also tested in 8 hour full immersion of BS 11846 Method B acidified salt water solution as seen in Figure 13c. Intergranular corrosion is visible in both the mixed and thermally cycled 6061 regions of the wedge. In the brazed wedge, there is additional Si along grain boundaries that likely affects IGC and pitting. In the mixed region there is nearly continuous intergranular corrosion along grain boundaries and Si along these grain boundaries is also visible (Figure 13c). IGC is worse in grain

boundaries that contain both Si and either β or Q phase as expected in this region based on thermodynamic and kinetic modeling (Figure 11).

SEM micrographs in backscattered and secondary electron image mode were taken to reveal the microstructure associated with each region. Figure 14 shows a backscattered electron image and EDS across a portion of the wedge gap. The Si rich and Al rich portions of the eutectic microstructure wtihin the braze gap were detected. Figure 15 shows the post- immersion micrographs of Region 1, the braze region. Slight corrosion of the Al rich portion of the eutectic can be detected in this region. In the braze zone, corrosion of Al rich region of the eutectic is seen in the Al-Si eutectic especially around the Si rich boundaries (Figure 15). Si supports pitting corrosion of the Al rich eutectic phase within the braze as will be discussed below in electrochemical analysis. Although β, Q, and θ (at low Mg contents) precipitates are thermodynamically possible in the Al rich eutectic region, there is no indication of any particular effect of these beyond the pitting of the Al rich portion of the eutectic microstructure shown in Figure 15.

Figure 16 illustrates a position near grain boundaries in Region 2 further away from the mixed zone. Table 5 shows that the composition is close to AA 6061 T6 with elevated levels of Si and reduced levels of Mg. Literature [13] and the thermodynamic and kinetic modeling performed indicate that matrix precipitates are either coherent Q phase or β (Mg_2Si). Coherent matrix precipitates have a preferred orientation within each grain and are typically 0.5 to 1 μm in length. Equilibrium Q phase or β (Mg_2Si) are formed at grain boundaries. There is also likely eutectically formed Si along grain boundaries at the interface of the mixed and AA 6061 zones, but much less as the distance away from the braze zone increases to about 125 μm (Figure 4). The post 8 hour full immersion testing micrographs (Figure 16, 17, and 18) show intergranular corrosion in boundary regions both with and without solidification structure containing eutectically formed Si at the grain boundaries in Regions 2 and 3. In the AA 6061 T6 region (Figure 18b), continuous intergranular corrosion occurs similarly to the thermally cycled, but unbrazed, AA 6061 sample (TCT6) as seen in Figure 13 (b), with additional pitting attack inside grains.

Electrochemical Analysis of Commercial AA 6061 after Aging

Electrochemical behavior of AA 6061 in 0.6 M NaCl solution was investigated using upward E-log i scans. Pitting and repassivation potentials on isolated AA 6061 did not change significantly after various aging heat treatments as seen in Table 6. This may be because significant amounts of Si, Cu, and Mg are collected at precipitate phases after all heat treatments or that Mg and (Si+Cu) are roughly offsetting. The effect of solid solution alloying on Al pitting (more noble potentials for Si and Cu combined with a less noble potential for Mg) may be roughly offsetting towards E_{pit} (E_{pit} Al – Si is more noble, E_{pit} Al-Cu is more noble, and E_{pit} Al-Mg is less noble) [40-43]. Moreover, constituent particles remain similar in all aged conditions [15, 40-44].

AA 6061 T4 and AA 6061 T6 electrochemical analysis indicate similar OCPs, which are on average -0.721 V_{SCE} and -0.710 V_{SCE} in aerated 0.6 M NaCl, respectively. The pitting potential of AA 6061 T4 in 0.6 M NaCl aerated condition was -0.683 V_{SCE}. The pitting potential of AA 6061 T6 in 0.6 M NaCl aerated condition was -0.699 V_{SCE}. As seen in Table 6, the average open circuit potentials and the average pitting potentials of all thermal conditions were within 30 mV of each other, while the average repassivation potentials were within about 50 mV in aerated 0.6 M NaCl solution.Similar trends were found when tests were conducted in the BS 11846 Method B solution. It is clear from these results that the electrochemistry of the deconstructed phases must be considered.

Electrochemical Analysis of Deconstructed Phases

Figure 19 reports the open circuit potentials (OCPs), anodic and cathodic polarization behavior in an aerated condition in two solutions: 0.6 M NaCl and 0.51 M NaCl + 12 mL 10.0 N HCl per liter, pH=1.2. Independent of either solution, Mg_2Si has the most active corrosion potential. Active phases compared to the Al-Mg-Si matrix are high purity Al, β (Mg_2Si) and S (Al_2CuMg). Si and Cu are both local cathodes [3, 6, 45] that may contribute to IGC and pitting experienced in 6xxx series aluminum alloys [13]. Replated Cu and elemental Si are known to be cathodes with Cu serving as a stronger

cathode for ORR than Si or Al_2Cu [3, 7, 45, 46]. In both 0.6 M NaCl and acidified 0.51 M NaCl solutions,Si and Cu are significantly cathodic to the AA 6061 matrix and its pitting potential, E_{pit} AA 6061 T6 SHTQ. Thus, it is likely that AA 6061 pits in the presence of both Si and Cu. S and β phases will be active, and therefore could corrode actively at grain boundaries. The behavior of Q phase ($Al_4Cu_2Mg_8Si_7$) was unavailable, but Al and Mg dealloying might be expected at which point the Al-Cu-Si IMC might rise in potential.

DISCUSSION

Influence of Intermetallic Phases on IGC

It is likely that β-Mg_2Si is formed on grain boundaries (Figure 11). It is clear that this phase is electrochemically active and exhibits a high dissolution rate, at least in acidic or neutral environments (Figure 20). The electrochemical behavior of ($Al_4Cu_2Mg_8Si_7$) is less certain. S-Al_2CuMg is a well-known active phase with an initial Al+Mg/Cu ratio of 3:1 [47-50]. In contrast, $Al_4Cu_2Mg_8Si$ has an initial ratio of Al+Mg/(Cu+Si) of 12:9, or is far less active on this basis. However, electrochemistry of intermetallic phases is far more complicated than estimates from stoichiometry and cannot be deciphered from simple rules of mixture [51]. The behavior of NiAl is an excellent example of a case where Al_2O_3 formation can prevail in acid environments while NiO or $Ni(OH)_2$ is formed on outer layers and controls alkaline dissolution [51]. Nevertheless there is strong evidence for IGC susceptibility in 6XXX alloys specifically when they contain grain boundary Q [6-8, 11, 13-15]. The presence of Si from brazing and Cu from alloying can trigger formation of this phase which is also promoted by the thermal cycle of brazing. IGC can result.

Region 1: Pitting and Uniform Corrosion

Preferrential corrosion of the Al rich phase of the eutectic mixture occurred in region one after the 8 hour immersion (Figure 14). The pitting and open circuit potentials of Al are highly anodic to the more noble cathodic Si rich portion of the eutectic substantiating that a microgalvanic couple develops (Figures

19 and 20). This microgalvanic couple between the Al and Si is sustained in both 0.6 M NaCl and 0.51 M NaCl + 12 mL 10.0 N HCl solutions where $E_{OCP\ Si} > E_{pit\ Al}$ (Figure 19). Therefore, the Al rich areas will pit and corrode near Si rich phases as seen in Figure 15.

The diffusion of Mg into Region 1 is also a consideration. The Mg content of the braze region increases by approximately 0.4 wt % during dip brazing. The lowest Mg content where β forms is at 0.1 wt % (640 K) and 0.3 wt % (550 K) respectively on the predicted equilibrium phase diagram. The formation of other phases in Region 1 in addition to β is confirmed by the CCT and TTT curves (Figure 9a, b). Q, β, and Si are possible in Region 1 through cooling and artificial aging of the AA 6061 T6 and AA 4047 foil joint. β can actively dissolve in both the aqueous environments tested here as seen in Figure 20 (0.6 M NaCl and acidified 0.51 M NaCl solutions). If Q phase tends to behave more like β and S phases, active dissolution of Q may occur. However, Figure 15 does not indicate a strong effect of these phases on the corrosion of the Al-Si eutectic. Moreover, the braze gap does not affect these results. This is because there is not enough Si removal to produce a Al - Si binary alloy with low enough Si levels to form a Al-Si solid solution instead of the Al-Si eutectic (Figure 6a and 13c).

Regions 2, 3, and 4: IGC and Pitting Corrosion

Region 4 of the wedge structures has a composition similar to that of AA 6061 The schematic for the microstructure of Regions 2 and 3 is shown in Figure 21. The matrix of AA 6061 contains coherent β and Q phase. β and Q phases are likely formed along grain boundaries (Figures 2a, 2b, 4, and 10-11). Moreover, the thermal cycling experienced during the brazing process enhances both grain boundary and matrix precipitation (Figure 2). If literature is correct [6-8, 13-15], there also may be a thin Cu film along these grain boundaries. Additional Q phase is formed with increased aging. The intergranular corrosion mechanism likely involves β and Q phase corrosion based on their anodic potential to the matrix assuming the Q phase ($Al_4Cu_2Mg_8Si_7$) behaves similar to the S phase which is not certain. Along grain boundaries, certainly β and, perhaps, Q phase would likely corrode. Svenningsen et al. [8] believes

that a Cu film exacerbates IGC and enables continuous IGC by providing a potential with respect to the Al rich precipitate free zone and the grain boundary Q phase. The formation of coarse Si along grain boundaries as shown in Figures 4, 12, 16 and 17 would be expected to exacerbate this process by providing another local cathode as shown in Figure 19 and 20. Coherent β and Q phase dissolution is a likely also the cause of matrix pitting in Region 4 (Figure 20).

SUMMARY

Grain boundary phase formation and subsequent intergranular corrosion (IGC) susceptibility depended critically on Al-Si-Mg-Cu composition and thermal history. IGC is speculated to be promoted by β and Q phase formation on grain boundaries where the latter was promoted by copper contents ranging from 0.2-0.5% as well as high Si levels. The Cu content in AA 6061 studied was within the range from 0.2-0.3 wt%. Grain boundary phases enabled IGC in both unbrazed AA 6061 T6 and AA 6061 T6 that experienced the brazing thermal cycle and was then reaged to T6 (TCT6). This is because grain boundary precipitation was exacerbated by both cooling from the braze cycle as well as subsequent isothermal aging. The Al-Si eutectic microstructure of the brazed zone undergoes predictable corrosion of the Al-rich phase as expected based on microgalvanic coupling. Brazing induces significant Si transport to distances of 125 micrometers into the precipitation age hardened Al-Mg-Si-Cu alloy and promoted formation of coarse resolidified Al-Cu-Mg grains. Moreover, a eutectically formed Al-Si microstructure formed at solidification boundaries upon cooling from the Si rich liquid. IGC occurred in the Al-Mg-Si-Cu alloy in these regions because of β and likely Q phase formation on grain boundaries as well as the presence of eutectically formed Si. Electrochemical tests confirmed the unfavorable micro-galvanic coupling relationship between grain boundary Mg_2Si relative to the Al-Cu-Mg alloy matrix, Cu, Theta and eutectically formed Si. Eutectically formed Si needles on grain boundaries also containing Beta and likely Q likely exacerbates the process of IGC by providing an additional local cathode.

ACKNOWLEDGEMENTS

This work was supported by the Office of Naval Research Grant No. N00014-06-1-0554 under the direction of Dr. D. Shifler. Coleman Microwave, in particular D. Braithwaite, is gratefully acknowledged for helpful support with brazing of the sandwich structures tested. Dr. H.N.G. Wadley-UVa Research Group; DOE Ames, Alcoa as well as Dr. N. Birbilis of Monash University are also gratefully acknowledged. R. White, F. Bovard, R. Holloman, Dr. J. Fitz-Gerald, and Dr. W. Soffa are thanked for technical and alloying assistance. J.W. McCarthy and L.E. Scully are also acknowledged for laboratory assistance.

REFERENCES

1. D.T. Queheillalt, Y. Murty, and H.N.G. Wadley, "Mechanical properties of an extruded pyramidal lattice truss sandwich structure," Scripta Mater S8, 1 (2008): p. 76.
2. E.B. Gempler, Brazing of Aluminum Alloys, in Welding, Brazing, and Soldering (ASM International: Materials Park, Ohio, 1993) p. 937.
3. A.K. Bhattamishra and K. Lal, "Microstructural studies on the effect of Si and Cr on the intergranular corrosion in Al-Mg-Si alloys," Materials Design 18, 1 (1997): p. 25.
4. T.D. Burleigh, "Microscopic Investigation of the Intergranular Corrosion of Alloy 6013-T 6," Sintef Metallurgy (1992): p. 435.
S. T.D. Burleigh, E.D. Ludwiczak, and R.A. Petri, "Intergranular corrosion of an aluminum-magnesium-silicon-copper alloy," Corrosion 51, 01 (199S).
6. M.H. Larsen, J.C. Walmsley, O. Lunder, R.H. Mathiesen, and K. Nisancioglu, "Intergranular Corrosion of Copper-Containing AA6xxx AlMgSi Aluminum Alloys," J Electrochem Soc 1S5, 11 (2008): p. CS50.
7. M.H. Larsen, J.C. Walmsley, O. Lunder, and K. Nisancioglu, "Effect of Excess Silicon and Small Copper Content on Intergranular Corrosion of 6000-Series Aluminum Alloys," J Electrochem Soc 1S7, 2 (2010): p. C61.
8. G. Svenningsen, M.H. Larsen, J.C. Walmsley, J.H. Nordlien, and K. Nisancioglu, "Effect of artificial aging on intergranular corrosion of extruded AlMgSi alloy with small Cu content," Corros Sci 48, 6 (2006): p. 1S28.
9. J.L. Murray and A.J. McAlister, Al-Si (Aluminum-Silicon), in Binary alloy phase diagrams, T.B. Massalski and H. Okamoto, eds. (ASM International: Materials Park, Ohio, 1990)
10. J.R. Scully, "Environment-assisted intergranular cracking," Mrs Bull 24, 7 (1999): p. 36.
11. M.H. Larsen, J.C. Walmsley, O. Lunder, and K. Nisancioglu, "Effect of Heat Treatment on Grain Boundary Nanostructure and Corrosion of Low Copper AlMgSi Alloy," ECS Transactions 3, 31 (2007): p. 167.
12. A. Shi, "Characterization of 6111-like aluminum alloys using electrochemical techniques and electron microscopy" (Ph.D. diss, University of Michigan: Ann Arbor, MI, 2003).
13. G. Svenningsen, M.H. Larsen, J.H. Nordlien, and K. Nisancioglu, "Effect of high temperature heat treatment on intergranular corrosion of AlMgSi(Cu) model alloy," Corros Sci 48, 1 (2006): p. 2S8.

14. G. Svenningsen, M.H. Larsen, J.H. Nordlien, and K. Nisancioglu, "Effect of thermomechanical history on intergranular corrosion of extruded AlMgSi(Cu) model alloy," Corros Sci 48, 12 (2006): p. 3969.
15. G. Svenningsen, J.E. Lein, A. Bjorgum, J.H. Nordlien, Y.D. Yu, and K. Nisancioglu, "Effect of low copper content and heat treatment on intergranular corrosion of model AlMgSi alloys," Corros Sci 48, 1 (2006): p. 226.
16. T.L. Su, S.S. Wang, L.C. Tsao, S.Y. Chang, T.H. Chuang, and M.S. Yeh, "Corrosion behaviors of Al-Si-Cu-based filler metals and 6061-T6 brazements," Journal of Materials Engineering and Performance 11, 2 (2002): p. 187.
17. H. Bart-Smith, J.W. Hutchinson, and A.G. Evans, "Measurement and analysis of the structural performance of cellular metal sandwich construction," Int J Mech Sci 43, 8 (2001): p. 1945.
18. R. Biagi, J.Y. Lim, and H. Bart-Smith, "In-Plane Compression Response of Extruded Aluminum 6061-T6 Corrugated Core Sandwich Columns," Journal of the American Ceramic Society 94, (2011): p. S76.
19. H.N.G. Wadley, "Multifunctional periodic cellular metals," Philos T Roy Soc A 364, 1838 (2006): p. 31.
20. J.R. Davis, Corrosion of aluminum and aluminum alloys (Materials Park, OH: ASM International, 1999). p. vii.
21. S. Kuroda, T. Itagaki, and K. Tohma, "Electrochemical property of Al–Si alloy brazing filler," Journal of Japan Institute of Light Metals 46, 3 (1996): p. 113.
22. D.J. Chakrabarti and D.E. Laughlin, "Phase relations and precipitation in Al-Mg-Si alloys with Cu additions," Progress in Materials Science 49, 3-4 (2004): p. 389.
23. D. Braithwaite, Coleman Microwave, correspondence to D. Braithwaite, (2008).
24. BS 11846, "Corrosion of metals and alloys. Determination of resistance to intergranular corrosion of solution heat- treatable aluminium alloys" 1996.
25. ASTM G1, "Standard Practice for Preparing, Cleaning, and Evaluating Corrosion Test Specimens" (West Conshohocken, PA: ASTM International, 2003).
26. J.O. Andersson and J. Agren, "Models for Numerical Treatment of Multicomponent Diffusion in Simple Phases," Journal of Applied Physics 72, 4 (1992): p. 1350.
27. Y. Du, Y.A. Chang, B.Y. Huang, W.P. Gong, Z.P. Jin, H.H. Xu, Z.H. Yuan, Y. Liu, Y.H. He, and F.Y. Xie, "Diffusion coefficients of some solutes in fcc and liquid Al: critical evaluation and correlation," Materials Science and Engineering a-Structural Materials Properties Microstructure and Processing 363, 1-2 (2003): p. 140.
28. R.J. Zhang, M. Li, and J. Allison, "Phase-field study for the influence of solute interactions on solidification process in multicomponent alloys," Comp Mater Sci 47, 3 (2010): p. 832.
29. N. Saunders and A.P. Miodownik, CALPHAD (calculation of phase diagrams) : a comprehensive guide. Pergamon materials series (Pergamon: Oxford; New York:, 1998). p. xvi.
30. A. Zhu, G.J. Shiflet, and E.A. Starke, Application of computational and experimental techniques in intelligent design of age-hardenable aluminum alloys in Applied Computational Materials Modeling, G. Bozzolo, R. D. Noebe, P. B. Abel, D. R. Vij, eds. (Springer US: New York, 2007) p. 307.
31. A.W. Zhu, S.J. Poon, and G.J. Shiflet, "On glass formability of Al-Gd-Ni (Fe)," Scripta Mater 50, 12 (2004): p. 1451.
32. M. Avrami, "Kinetics of Phase Change. I General Theory," The Journal of Chemical Physics 7, 12 (1939): p. 1103.
33. M.H. Jacobs, "The structure of the metastable precipitates formed during ageing of an Al-Mg-Si alloy," Philos Mag 26, 1 (1972): p. 1.

34. J.M. Silcock, T.J. Heal, and H.K. Hardy, "Structual Ageing Characteristics of Binary Aluminum-Copper Alloys," Journal Institute of Metals 82, (1954): p. 239.
35. P. Villars and L.D. Calvert, Pearson's Handbook of Crystallographic Data for Intermetallic Phases. Vol. II (Materials Park, OH: ASM International, 1991). p. 2639.
36. J.W. Cahn, "Nucleation on dislocations," Acta Metall Mater 5, 3 (1957): p. 169.
37. J.D. Robson, M.J. Jones, and P.B. Prangnell, "Extension of the N-model to predict competing homogeneous and heterogeneous precipitation in Al-Sc alloys," Acta Materialia 51, 5 (2003): p. 1453.
38. D. Turnbull, "Formation of crystal nuclei in liquid metals," Journal of Applied Physics 21, 10 (1950): p. 1022.
39. ASTM B918/B918M, "Standard Practice for Heat Treatment of Wrought Aluminum Alloys", (West Conshohocken, PA: ASTM International, 2003).
40. E. Brillas, P.L. Cabot, F. Centellas, J.A. Garrido, E. Perez, and R.M. Rodriguez, "Electrochemical oxidation of high-purity and homogeneous Al-Mg alloys with low Mg contents," Electrochim Acta 43, 7 (1998): p. 799.
41. I.L. Muller and J.R. Galvele, "Pitting potential of high purity binary aluminium alloys—I. Al-Cu alloys. Pitting and intergranular corrosion," Corros Sci 17, 3 (1977): p. 179.
42. I.L. Muller and J.R. Galvele, "Pitting potential of high purity binary aluminium alloys—II. AlMg and AlZn alloys," Corros Sci 17, 12 (1977): p. 995.
43. H. Yoshioka, S. Yoshida, A. Kawashima, K. Asami, and K. Hashimoto, "The Pitting Corrosion Behavior of Rapidly Solidified Aluminum-Alloys," Corros Sci 26, 10 (1986): p. 795.
44. T. Aburada, Effects of Minor Solute on Corrosion, (Ph.D. diss., Univ. of Virginia: Charlottesville, VA, 2011).
45. J.R. Scully, D.E. Peebles, A.D. Romig, D.R. Frear, and C.R. Hills, "Metallurgical Factors Influencing the Corrosion of Aluminum, Al-Cu, and Al-Si Alloy Thin-Films in Dilute Hydrofluoric Solution," Metall Trans A 23, 9 (1992): p. 2641.
46. J.R. Scully, T.O. Knight, R.G. Buchheit, and D.E. Peebles, "Electrochemical Characteristics of the Al2cu, Al3ta and Al3zr Intermetallic Phases and Their Relevancy to the Localized Corrosion of Al-Alloys," Corros Sci 35, 1-4 (1993): p. 185.
47. R.G. Buchheit, R.P. Grant, P.F. Hlava, B. Mckenzie, and G.L. Zender, "Local dissolution phenomena associated with S phase (Al2CuMg) particles in aluminum alloy 2024-T3," Journal of the Electrochemical Society 144, 8 (1997): p. 2621.
48. R.G. Buchheit, L.P. Montes, M.A. Martinez, J. Michael, and P.F. Hlava, "The electrochemical characteristics of bulk-synthesized Al2CuMg," Journal of the Electrochemical Society 146, 12 (1999): p. 4424.
49. G.O. Ilevbare, O. Schneider, R.G. Kelly, and J.R. Scully, "In situ confocal laser scanning microscopy of AA 2024-T3 corrosion metrology - I. Localized corrosion of particles," J Electrochem Soc 151, 8 (2004): p. B453.
50. O. Schneider, G.O. Ilevbare, J.R. Scully, and R.G. Kelly, "In situ confocal laser scanning microscopy of AA 2024-T3 corrosion metrology - II. Trench formation around particles," J Electrochem Soc 151, 8 (2004): p. B465.
51. R.S. Lillard and J.R. Scully, "Electrochemical passivation of ordered NiAl," Journal of the Electrochemical Society 145, 6 (1998): p. 2024.

TABLES AND FIGURES

Table 1. Composition of test UNS A96061 (AA 6061) and UNS A94047 (Al-Si alloy) brazing sheet material.

Alloy	Nominal composition (wt%)									
	Al	Mg	Si	Cu	Fe	Mn	Cr	Zn	Ti	Other
UNS A96061 (AA 6061) T4 *	97.52	1	0.58	0.2	0.3	0.13	0.12	0.08	0.04	0.03
UNS A96061 (AA 6061) T6 †	97.41	0.85	0.64	0.22	0.48	0.1	0.18	0.04	0.06	0.02
UNS A94047 (AA 4047, BAlSi-4) ‡	balance	0.1 max	11 to 13	0.3 max	0.8 max	0.15 max	-	0.02 max	-	0.15

* AA 6061 T4 actual composition with sheet thickness in S direction of = 4.83 mm, plate size 4.83 mm x 1219 mm x 2438 mm.
† AA 6061 T6 actual composition with sheet thickness in S direction of = 4.78 mm, plate size 4.78 mm x 1219 mm x 3658 mm.
‡ Reported range for filler foil material, exact composition is not known.

Table 2. Parameters used for modeling for equilibrium phases considered at grain boundaries†.

Phase	Nominal Composition	Unit Cell	V (per atom)
β†,[31]	Mg_2Si	FCC a =0.639 nm	0.022 nm^3
Si	Si	Diamond cubic a =0.543 nm	0.020 nm^3
θ[32]	Al_2Cu	Body centered tetragonal a = b = 0.607 nm c = 0.487 nm	0.015 nm^3
Q‡,[33]	$Al_5Cu_2Mg_8Si_6$[26]	Hexagonal a = 1.04 nm c = 0.405 nm	0.021 nm^3
S[29]	Al_2CuMg	Side-centered orthorhombic a = 0.401 nm b = 0.935 nm c=0.715 nm	0.020 nm^3

† GP, β", β' and β have different crystal structures but the same composition.
‡ Q', and Q have the same structure, lattice parameter and composition.

Table 3. Compositions of alloys utilized for CALPHAD modeling based on actual compositions reported by manufacturer for sheet procured, AA 6061 T6 and AA 4047 filler foil.

Alloys	Elements (wt%)			
	Al	Mg	Si	Cu
AA 6061 (UNS A96061)	Balance	0.9	0.6	0.2
AA 4047 [BAlSi-4] (UNS A94047)	Balance	0.1	13	0.3

Table 4. Parameters used in TTT and CCT calculations for total energy to form a nucleus on grain boundaries.

	Al	Cu	Mg	Si	Q-phase	β-phase
μ, (GPa)	26	48	17	17	22	17
n	0.35	0.34	0.29	0.42	0.35	0.33
strain-misfit					0.05	0.05
DG_e, (J/atom)					$1.07x10^{-21}$	$9.66x10^{-22}$

Table 5. Summary of expected equilibrium phases in each region of a UNS A96061 joint brazed with UNS A94047 and reheated to the T6 condition based on composition deduced from transport modeling assuming homogeneous precipitation and in some cases confirmed by experimental observations.

Braze Transport Region	Composition (wt%)	Phases Expected after CCT and TTT*
1 - Pre braze	Al balance, 0.1Mg, 13Si, 0.3Cu	Eutectic Al–Si microstructure, precipitated Si, Q, θ in Al-rich phase
1 – Post braze	Al balance, 0.49 Mg, 5.51Si, 0.3Cu	Eutectic Al-Si microstructure, precipitated Si, Q, β in Al-rich phase
2 – Post braze	Al balance, 0.5 Mg, 4.8 Si, 0.2 Cu	Eutectic Al-Si microstructure at solidifcation boundaries, precipitated Si, Q, β in Al-rich phase
3 – Post Braze	Al balance, 0.62 Mg, 4.68 Si, 0.2 Cu	Eutectic Al-Si microstructure at solidication boundaries, precipitated, Q, β in Al matrix, Si precipitates
4 - Pre braze	Al balance, 0.9Mg, 0.6Si, 0.2 Cu	Al matrix with Q and β precipitates
4 – Post Braze	Al balance, 0.72Mg, 1.46Si, 0.2Cu	Al matrixwith Q, β, Si precipitates

* Based on thermodynamics and homogeneous kinetics. If a phase is available based on the phase diagram but not from kinetics, then the phase is not listed.

Table 6. Summary of average open circuit, pitting, and repassivation potentials for various thermal conditions of isolated UNS A96061 (AA 6061) sheet in aerated 0.6 M NaCl solution at 25°C.

Sample Type	OCP* avg (mV vs. SCE)	E_{pit}† avg (mV vs. SCE)	E_{repass}‡ avg (mV vs. SCE)	OCP stdev ± mV	E_{pit} stdev ± mV	E_{repass} stdev ± mV
AA 6061 T4	-721	-683	-933	8	3	1
AA 6061 T6	-710	-699	-956	4	3	8
AA 6061 Overaged #1	-730	-704	-975	15	5	6
AA 606 Overaged #2	-722	-694	-942	4	5	1
AA 6061 T6 Thermal Cycle to reT4 (TCT4)	-704	-677	-924	5	14	6
AA 6061 T6 Thermal Cycle to reT6 (TCT6)	-733	-680	-934	14	18	9
AA 6061 T6 SHTQ	-707	-679	-931	7	6	45

* OCP at the end of an 1800 second hold.

†, ‡ E_{pit} and E_{repass} determined at 10^{-4} A/cm^2

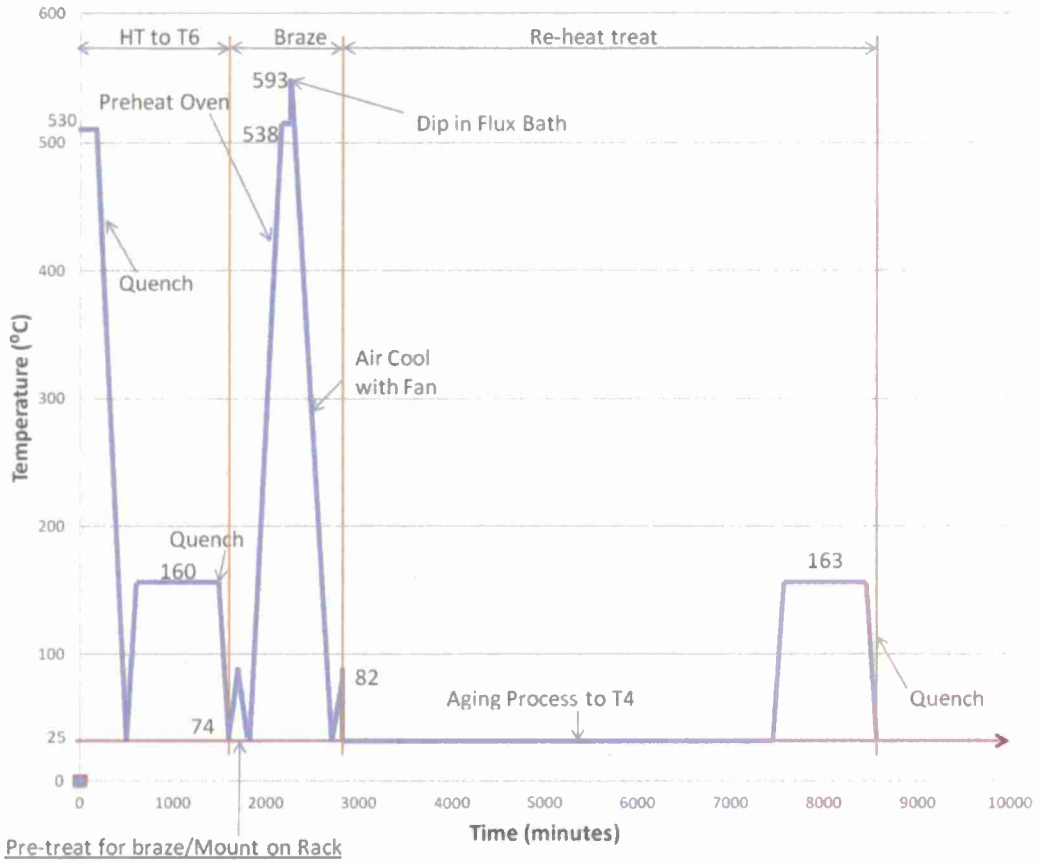

Figure 1. Thermal cycle of a dip brazed UNS A96061 (AA 6061) T6 extrusion with UNS A96061 (AA 6061) T6 face plates. The final processing step is either an air quench or fan air quench to ambient temperature.

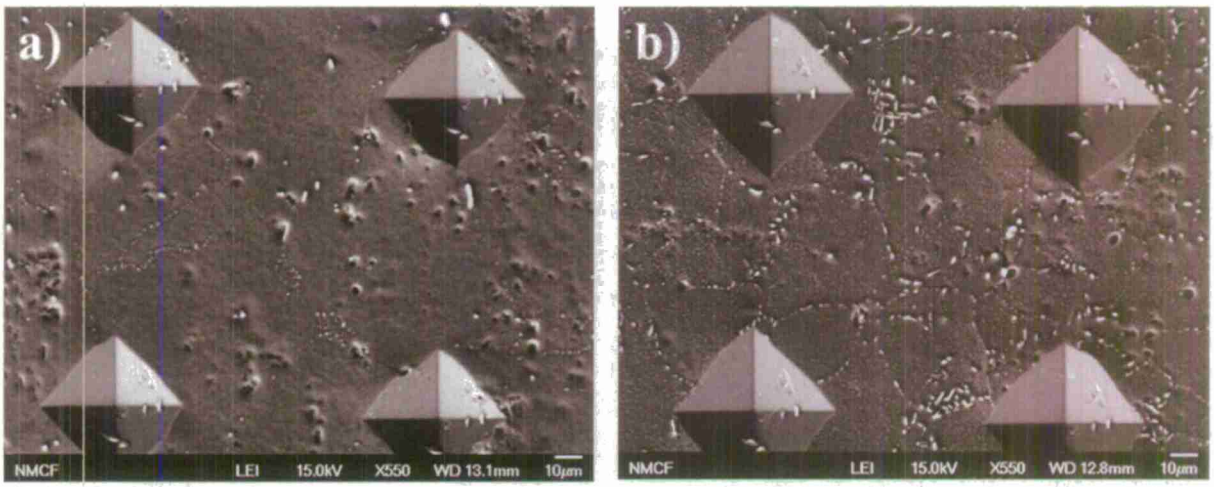

Figure 2. Scanning electron microscope secondary electron image (SEI mode) of mechanically polished and electropolished under the following thermal conditions **a)** UNS A96061 T6 and **b)** UNS A96061 T6 Thermal Cycle of Figure 1 and reaged to T6 (TCT6) conditions.

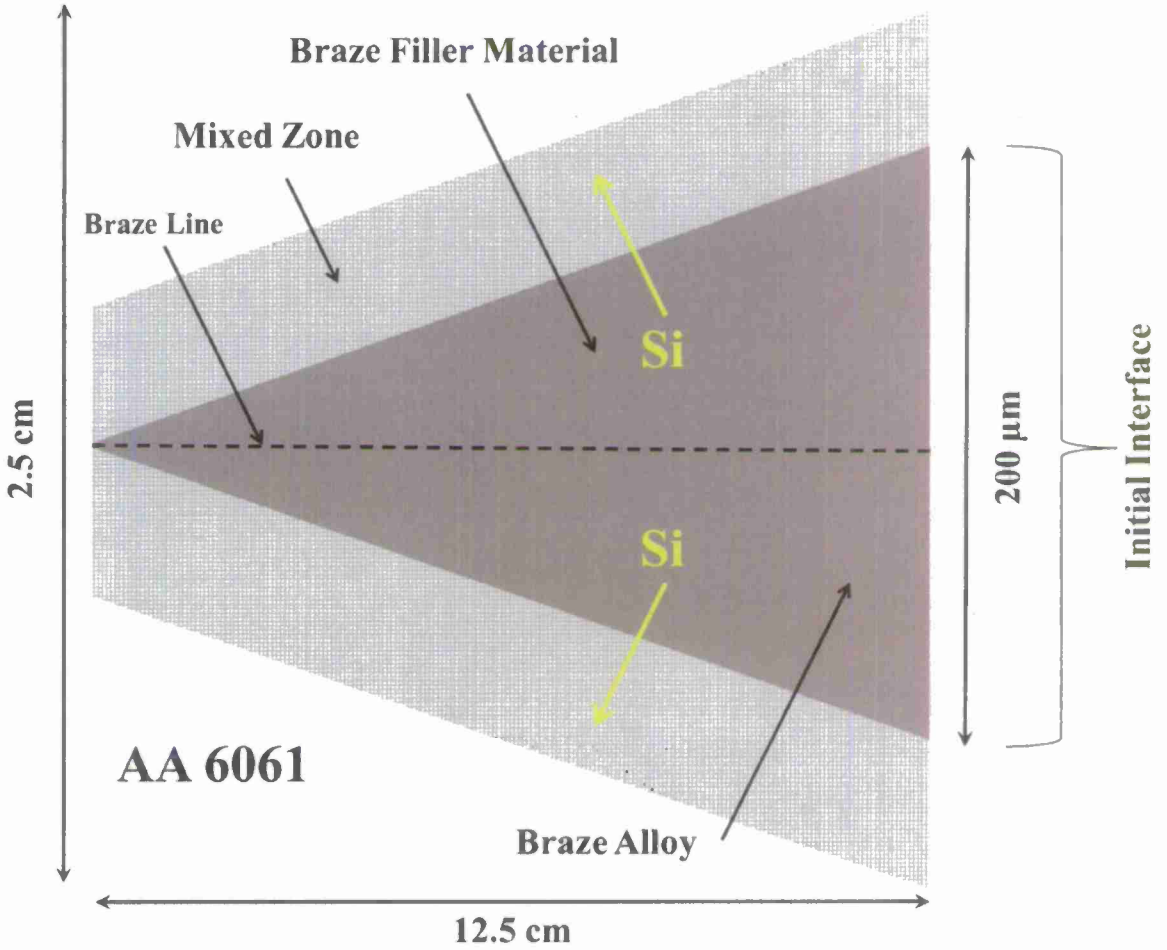

Figure 3. Wedge design with varying braze gap - schematic showing the effect of Si diffusion outward from the filler foil for an UNS A96061 T6 + UNS A94047 (BAlSi-4) filler foil wedge braze joint.

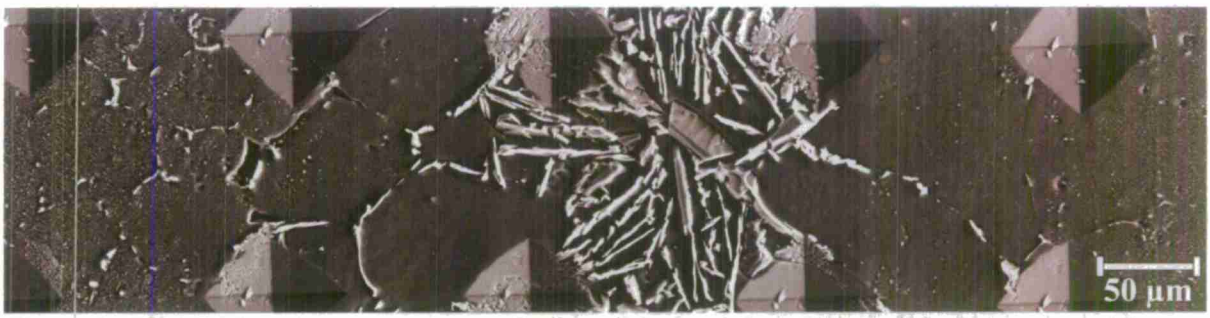

Figure 4. SEM (LEI mode) across a mechanically polished and then electropolished braze gap with a moderate to large gap wedge consisting of UNS A96061 T6 + UNS A94047 (BAlSi-4) filler foil reaged to T6 temper. Vickers indentation markers were used as reference points.

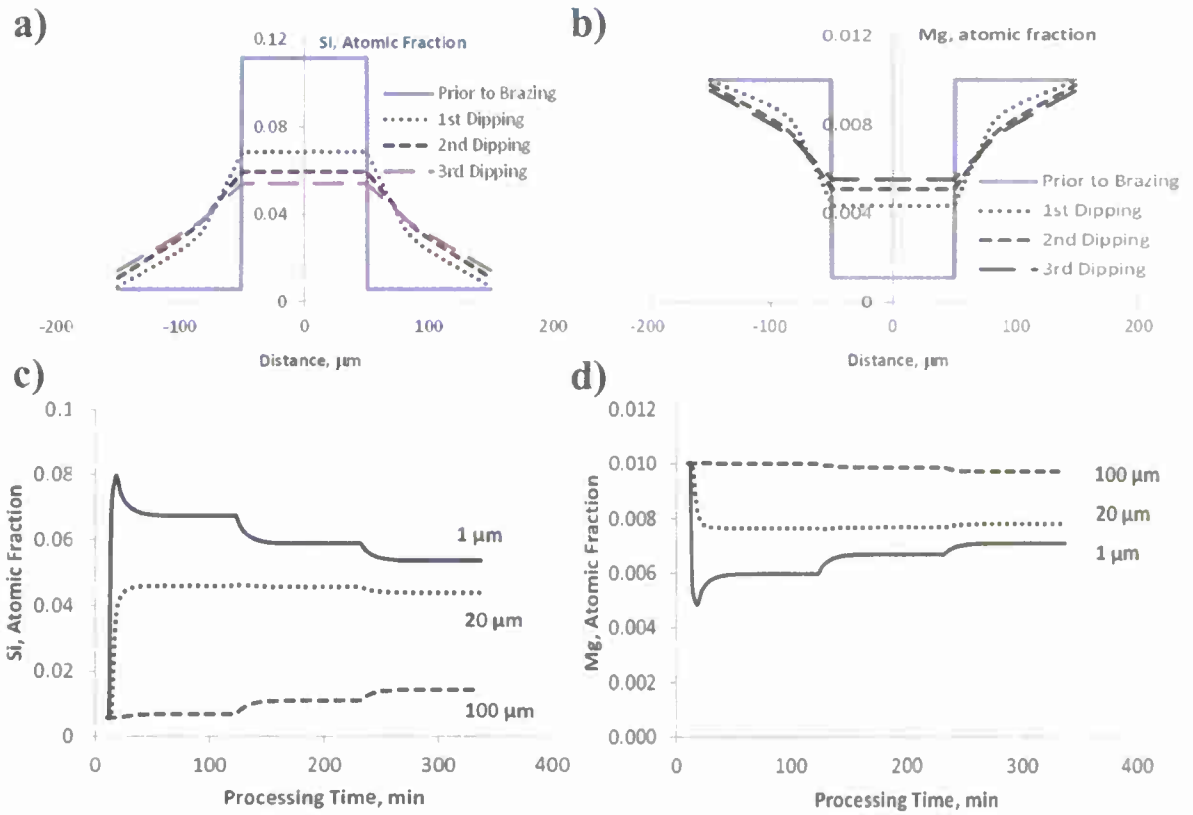

Figure 5. Model predicted: composition vs. distance plots assuming 100 μm foil thickness, 0.08 K/s cooling rate from 593^{0}C and perpendicular transport into a semi-infinite UNS A96061 plate. a) Si (atomic fraction) enrichment of the area surrounding the braze gap from the time prior to brazing until the third dip into the flux bath for brazing at various distances from the braze gap. b) Mg (atomic fraction) depletion from the zone surrounding the braze gap from the time prior to brazing until after the third dip into the flux bath for brazing. c) Si (atomic fraction) depletion with each successive dip into flux at 1, 20, and 100 μm positions from the braze and UNS A96061 T6 interface. d) Mg (atomic fraction) depletion/enrichment with each successive flux dip into flux at 1, 20, and 100 μm positions from the braze and UNS A96061 T6 interface.

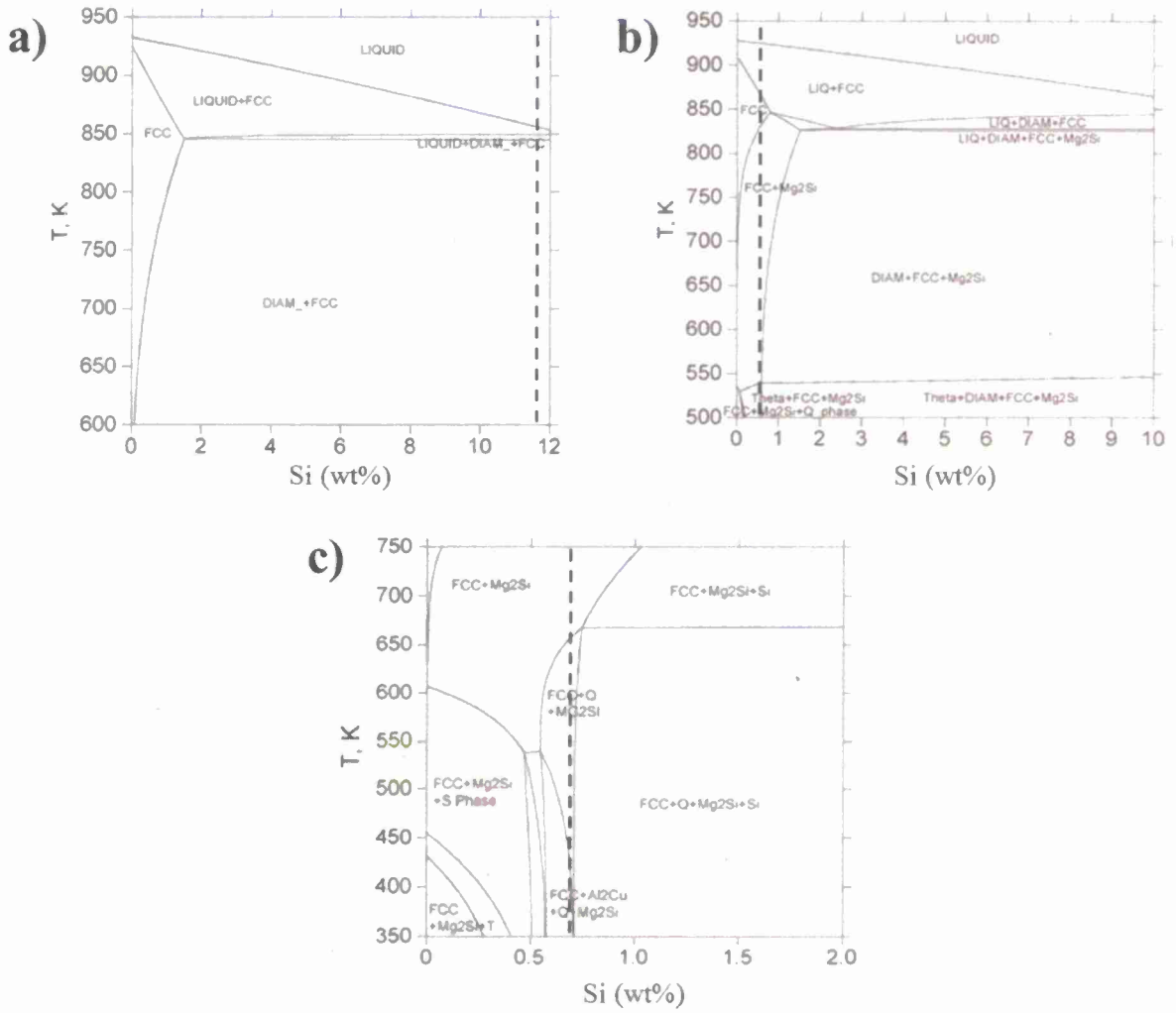

Figure 6. Phase diagrams calculated using CALPHAD approach a) UNS A94047 (BAlSi-4) representing the foil **before** brazing (Al balance, 0.3 wt% Mg, 0-12 wt% Si, 0.0 wt% Cu). b) UNS A96061 **before** brazing (Al balance, 1 wt% Mg, 0-10 wt% Si, 0.3 wt% Cu). c) UNS A96061 **after** brazing (Al balance, 1 wt% Mg, 0-2.0 wt% Si, 0.3 wt% Cu). The phases indicated are Mg_2Si (β), Al_2Cu (θ), T (Al_2MgSi), S (Al_2CuMg), Si (diamond), Al solid solution (FCC), Q ($Al_4Cu_2Mg_8Si_7$). Overall compositions of the alloys indicated are highlighted by the dotted line.

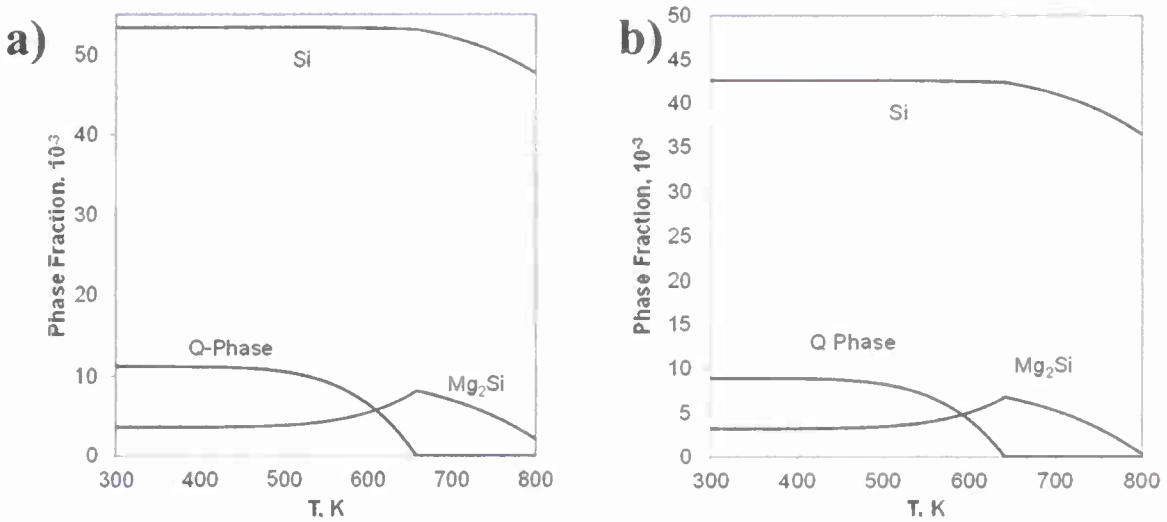

Figure 7. Predicted volume fractions of equilibrium phases as a function of temperature. Transition from Region 1 to 2. a) Region 2 **after** brazing, UNS A96061 + Si – Mg composition: Al balance, 0.6 wt% Mg, 6 wt % Si, 0.25 wt% Cu. b) Region 2 **after** brazing, UNS A96061 + Si – Mg composition: Al balance, 0.5 wt % Mg, 4.8 wt% Si, 0.2 wt % Cu.

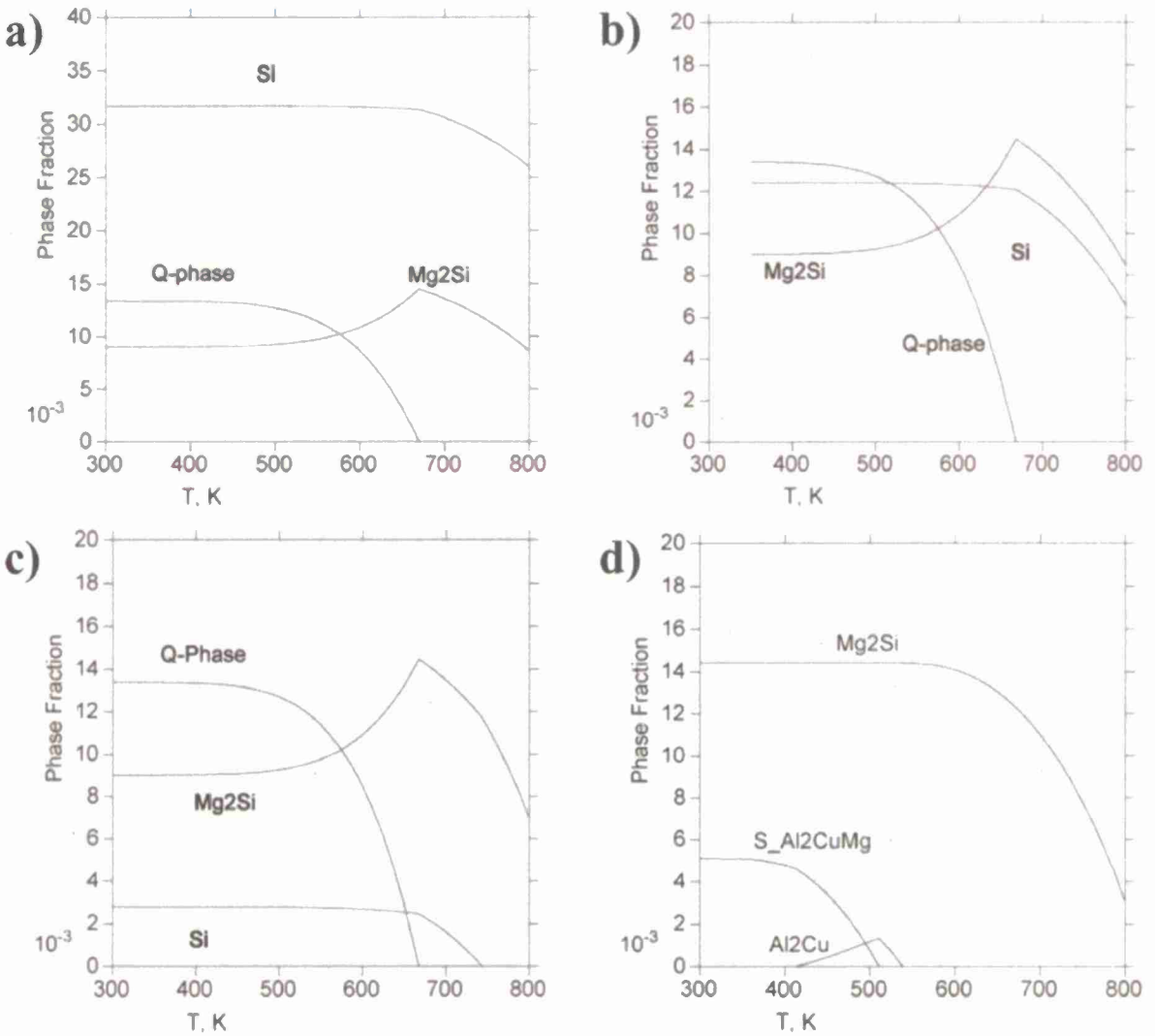

Figure 8. Predicted volume fractions of equilibrium phases as a function of temperature showing the transition from Region 3 to 4. a) Region 3 composition, Al balance, 1 wt% Mg, 4 wt % Si, 0.3 wt % Cu. b) Region 3/4 composition, Al balance, 1 wt% Mg, 2 wt % Si, 0.3 wt % Cu. c) Region 4 composition at slightly greater than 100 μm from the initial foil/ AA 6061 interface, Al balance, 1 wt% Mg, 1 wt % Si, 0.3 wt % Cu. d) Region 4, UNS A96061 low Si composition near commercial levels: Al balance, 0.3 wt% Cu, 1 wt% Mg, 0.5 wt% Si.

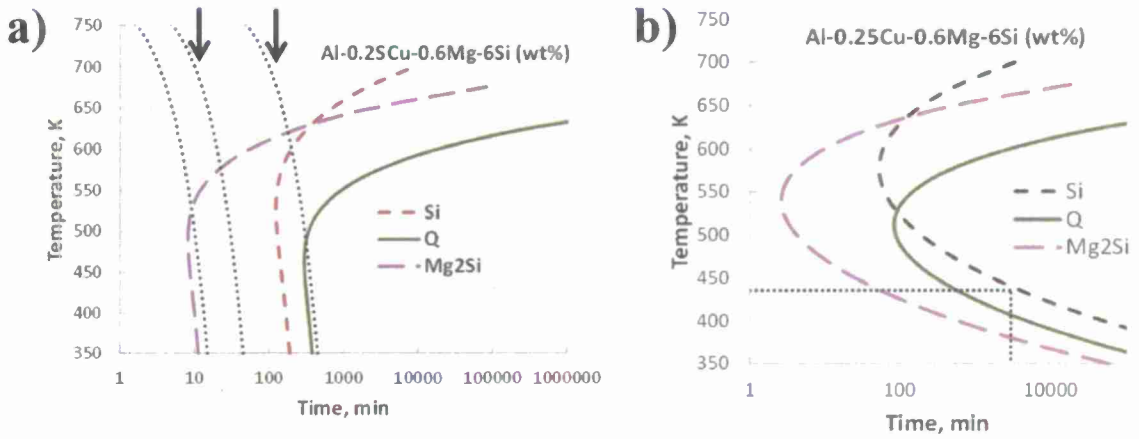

Figure 9. Continuous cooling curves and time temperature transformation curves based on homogeneous nucleation in the Al-Mg-Si-Cu alloy compositions indicated for transition from Region 1 to Region 2 **after** brazing. a) Region 1/2 CCT. b) Region 1/2 TTT. c) Region 2 CCT. d) Region 2 TTT. Si phase is precipitated Si. Dotted lines, from left to right in a), indicate cooling rates of 500 K/min, 50 K/min and 5 K/min. The cooling rates of interest for dip brazing are 50 K/min and 5k/min and are indicated by the vertical arrows.

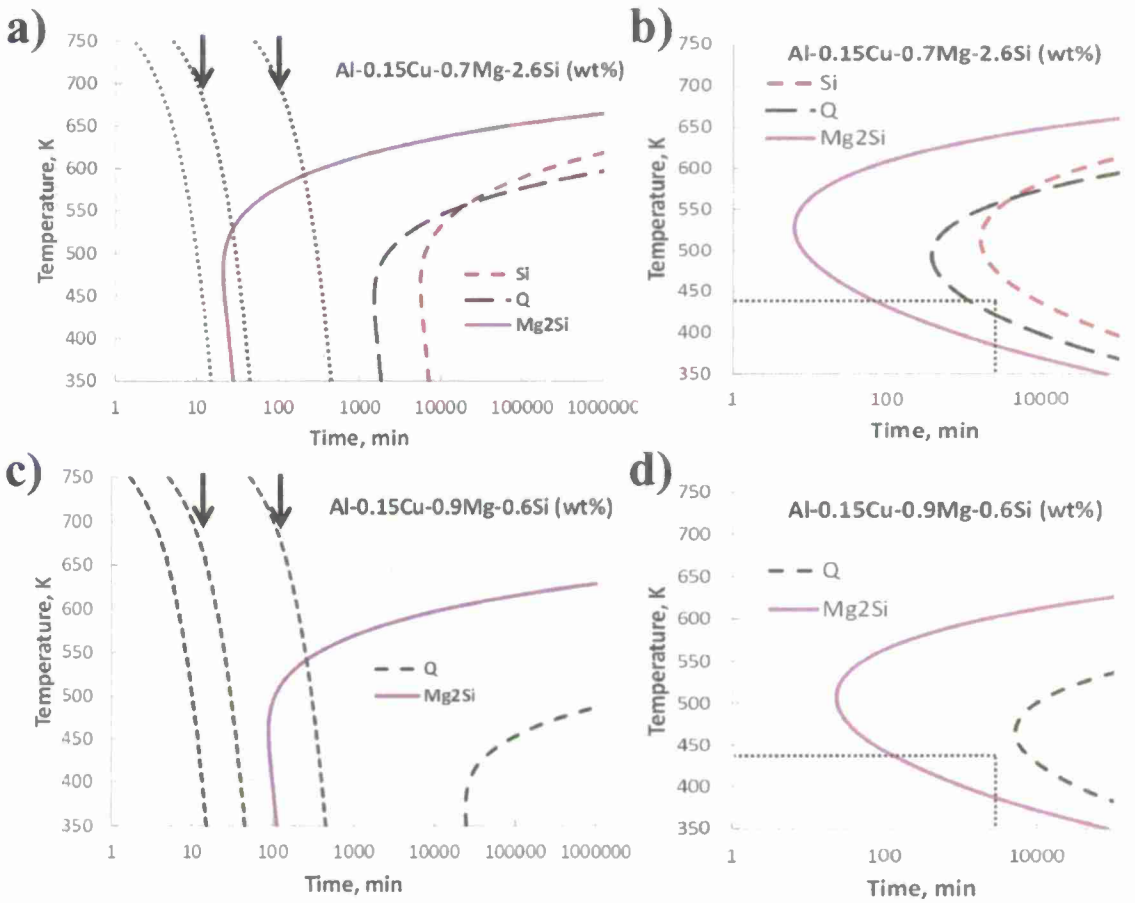

Figure 10. Continuous cooling curves and time temperature transformation curves based on homogeneous nucleation in the Al-Mg-Si-Cu alloy compositions indicated for Region 3/4 **after** brazing. a) Region 3 CTT, UNS A96061 + Si-Mg. b) Region 3 CCT, AA 6061 + Si-Mg. c) Region 4 CCT, UNS A96061. d) Region 4 TTT, UNS A96061. Si phase is precipitated Si. Cooling rates (dotted lines in a and c) of interest for dip brazing are 50 K/min and 5K/min are indicated by the vertical arrows.

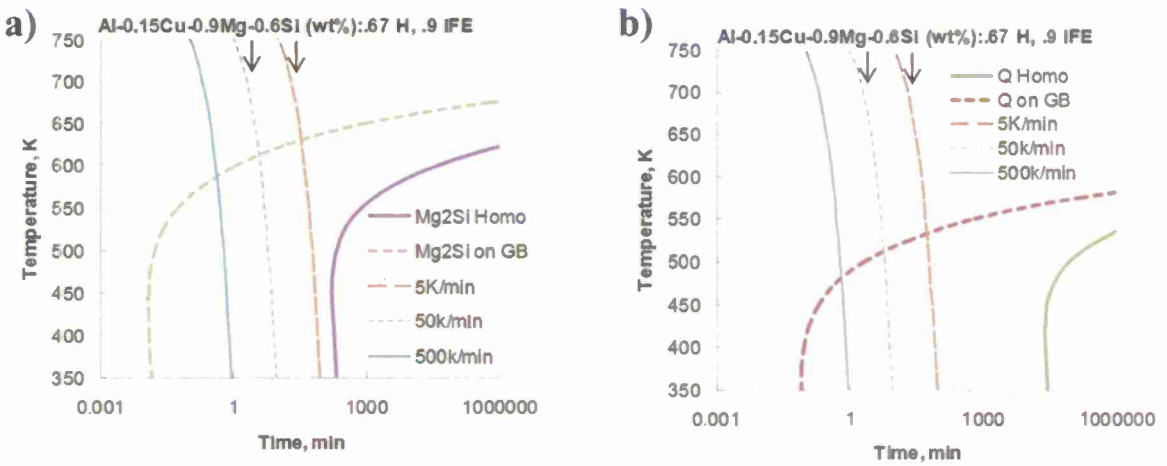

Figure 11. CCT curves assuming heterogeneous nucleation for phases on Q and β grain boundaries (for the alloy with Al balance, 0.15 wt% Cu, 0.7 wt% Mg, 2.6 wt% Si) with 33% reduced diffusion energy and 10% reduced interfacial energy. Cooling rates of interest for dip brazing are 5K/min and 50 K/min are indicated by the vertical arrows. UNS A96061 CCT and TTT curves are omitted because of their similarities to these CCT curves for Q and β. TTT curves are in agreement with CCT curves but are not shown for brevity.

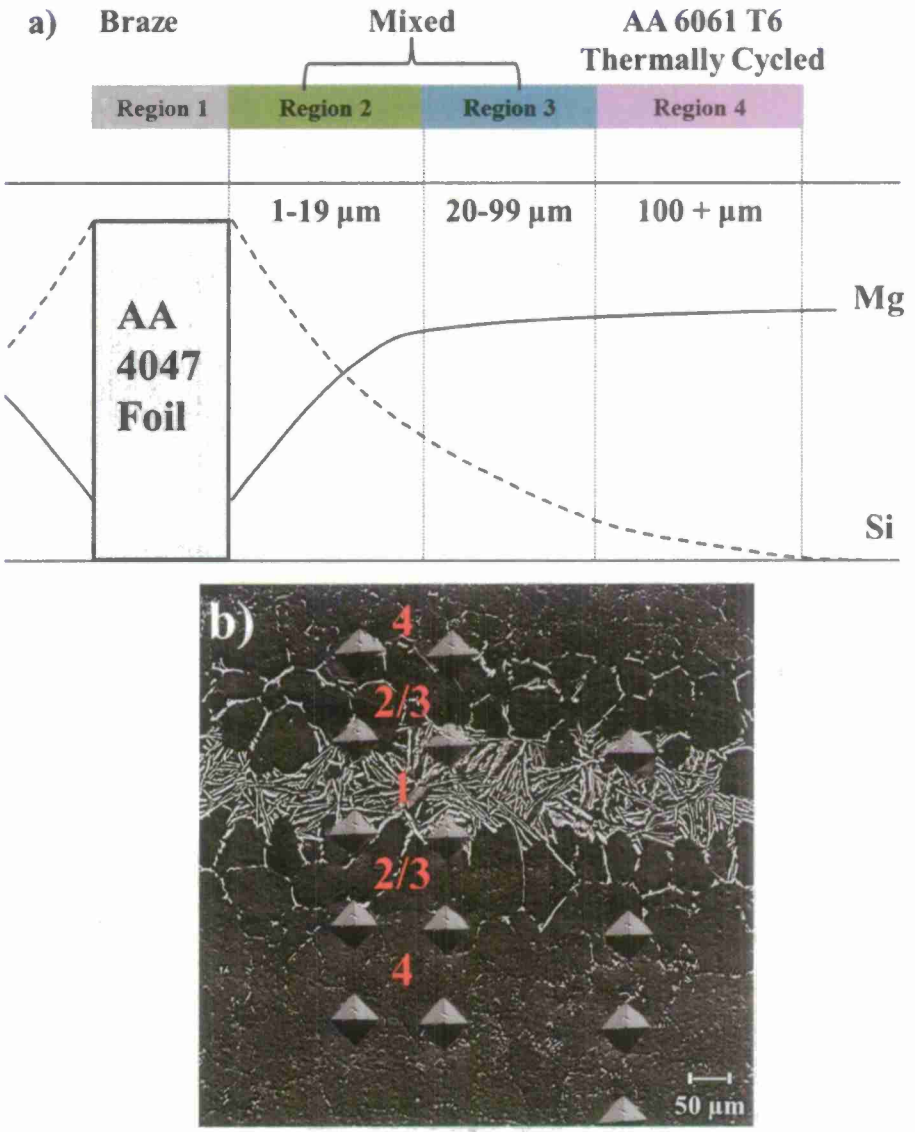

Figure 12. **a)** Schematic and **b)** corresponding micrograph of Regions 1 through 4 as defined by the distance from the original, unbrazed interface of UNS A96061 T6 and AA 4047 (BAlSi-4) filler foil.

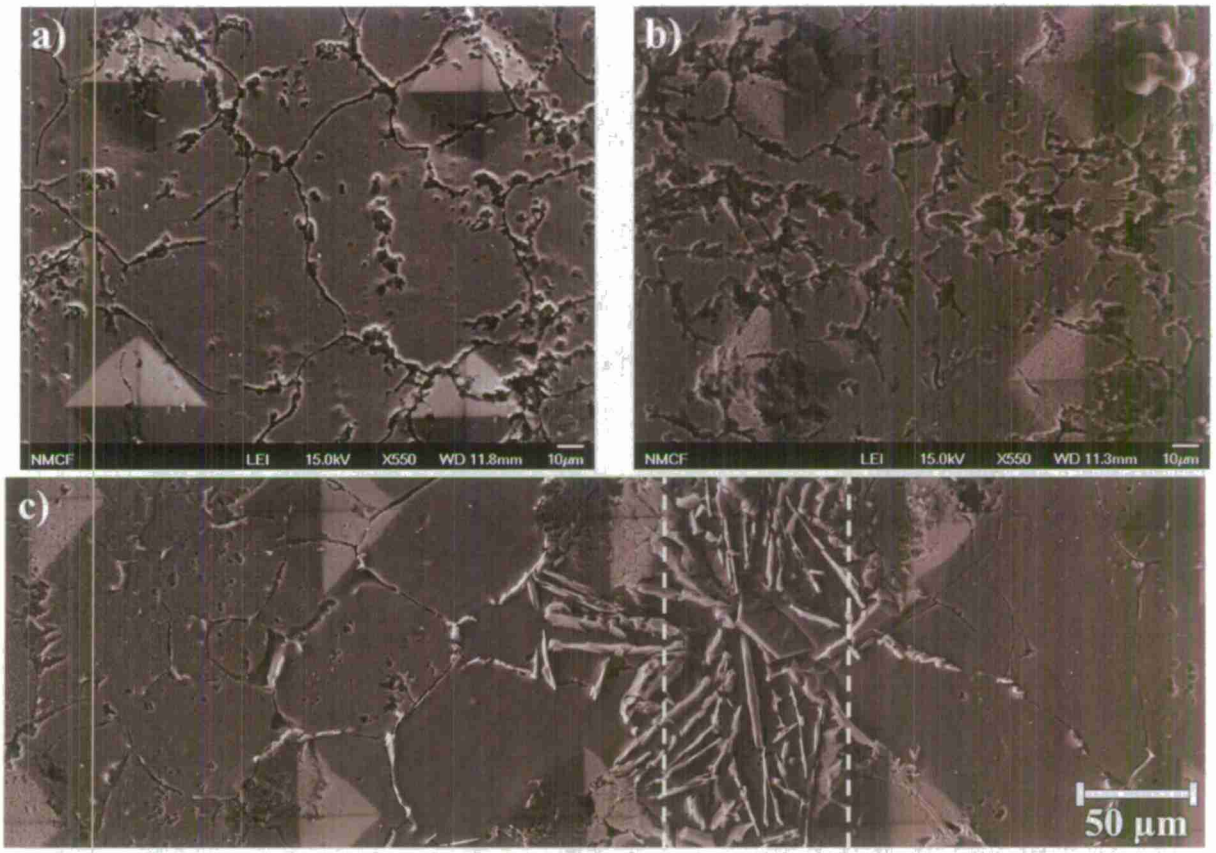

Figure 13. SEM micrographs of mechanically polished, electropolished thermal conditions exposed to acidified salt water for 8 hour full immersion testing at a) UNS A96061 T6 and b) UNS A96061 T6 Thermal Cycle and reaged to T6 (TCT6) condition. c) UNS A96061 T6 + UNS A94047 foil wedge.

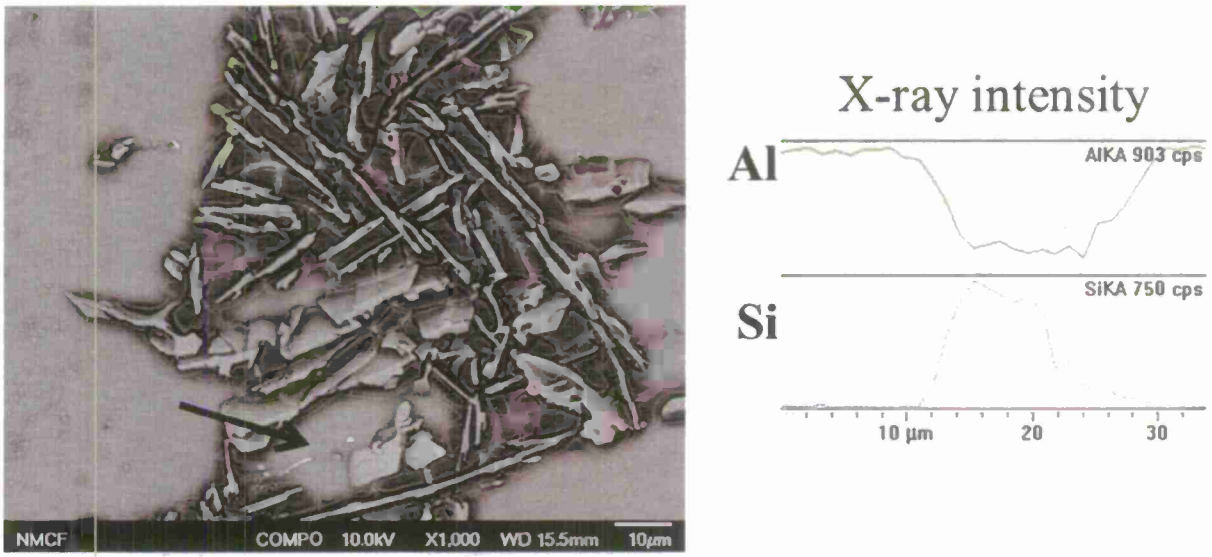

Figure 14. SEM (COMPO mode) of UNS A96061 T6 + UNS A94047 (BAlSi-4) wedge braze gap reheat treated to T6. SEM image and EDS line profile across eutectic microstructure (indicated by solid arrow) of the mechanically polished and electropolished wedge sample.

Figure 15. Region 1 (braze) UNS A96061 T6 + UNS A94047 (BAlSi-4) wedge reheat treated to T6. Shown is a post immersion micrograph of an initially mechanically polished and electropolished sample that was SEM imaged and then mechanically polished 5 μm. This sample was immersed for 8 hour immersion test in acidified salt water (BS 11846 Method B solution), cleaned and imaged.

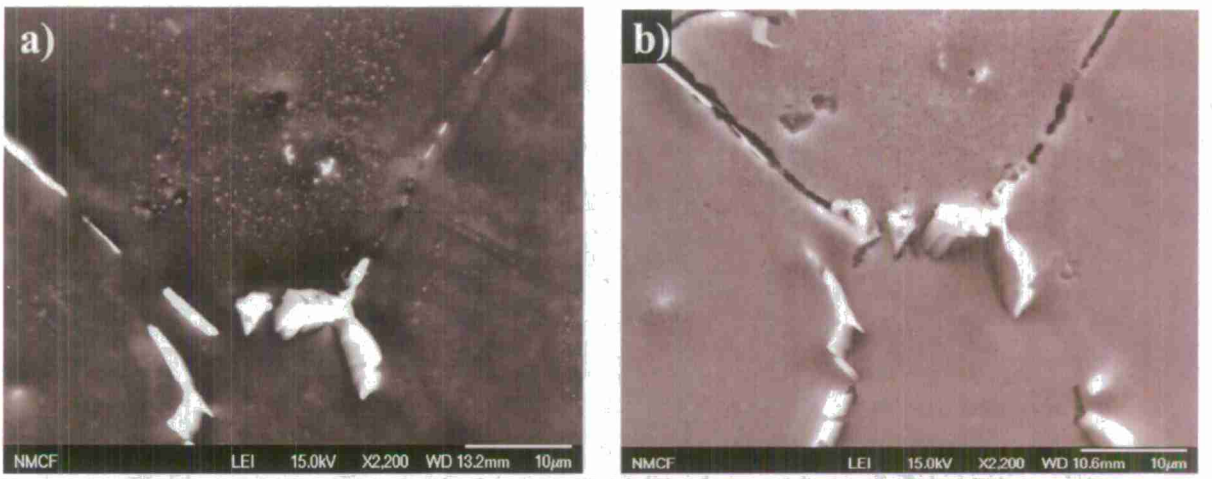

Figure 16. Region 2 (UNS A96061 + Si – Mg); UNS A96061 T6 + UNS A94047 (BAlSi-4) wedge reheat treated to T6; **a)** mechanically polished and electropolished sample prior to 8 hour immersion test in acidified salt water (BS 11846 Method B solution) **b)** mechanically polished 5 μm after initial SEM imaging, immersed for 8 hour immersion test in acidified salt water (BS 11846 Method B solution), cleaned, and imaged.

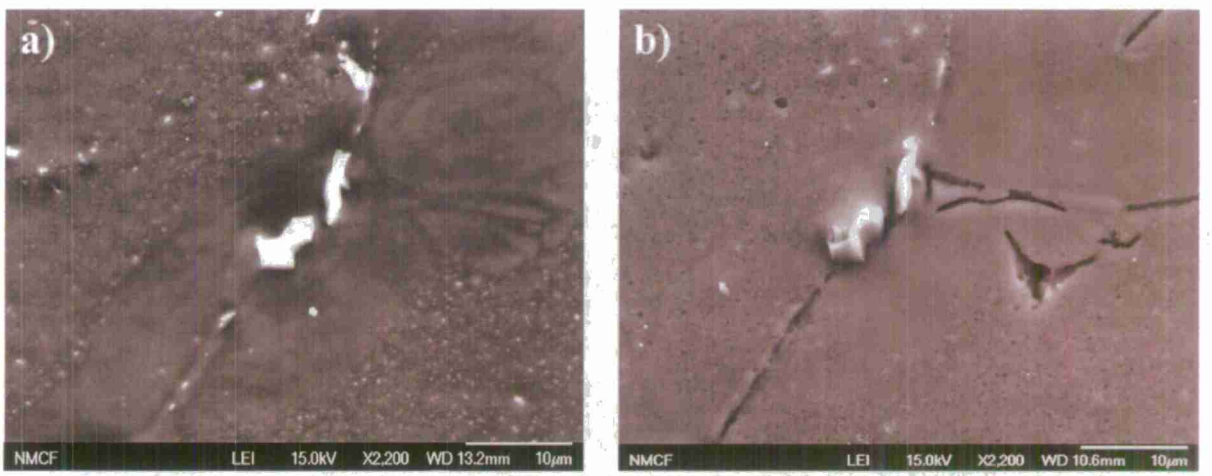

Figure 17. Region 3 (AA 6061 + Si – Mg); UNS A96061 T6 + UNS A94047 (BAlSi-4) wedge reheat treated to T6; **a)** mechanically polished and electropolished sample prior to 8 hour immersion test in acidified salt water (BS 11846 Method B solution) **b)** mechanically polished 5 μm after initial SEM imaging, immersed for 8 hour immersion test in acidified salt water (BS 11846 Method B solution), cleaned and imaged.

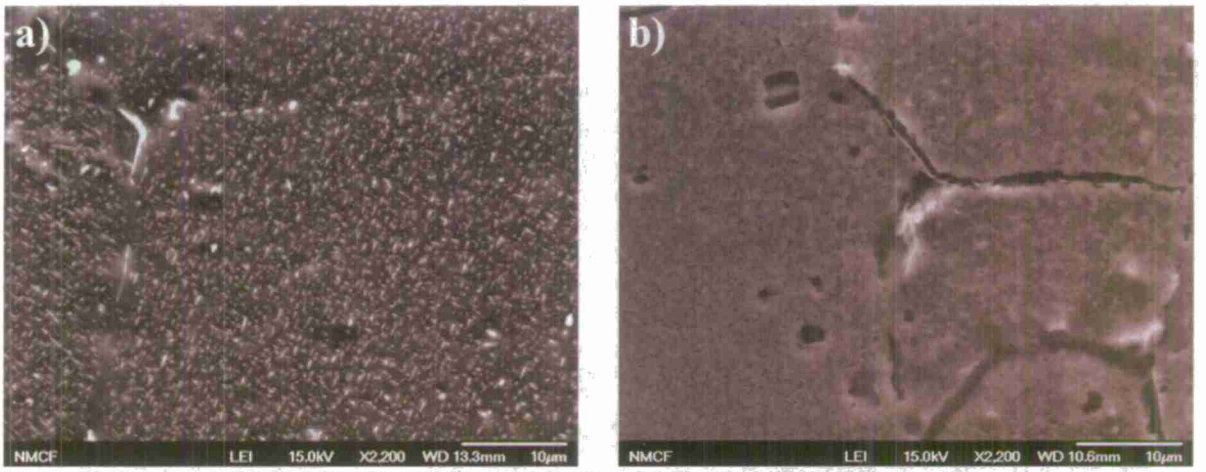

Figure 18. Region 4 (UNS A96061); UNS A96061 T6 + UNS A94047 (BAlSi-4) wedge reheat treated to a T6 condition; a) mechanically polished and electropolished sample prior to 8 hour immersion test in acidified salt water (BS 11846 Method B solution) b) mechanically polished 5 μm after initial SEM imaging, immersed for 8 hour immersion test in acidified salt water (BS 11846 Method B solution), cleaned, and imaged. Region 4 UNS A96061 T6 + UNS A94047 (BAlSi-4) reheat treated to T6 wedge. Exact positions unavailable for post corrosion testing.

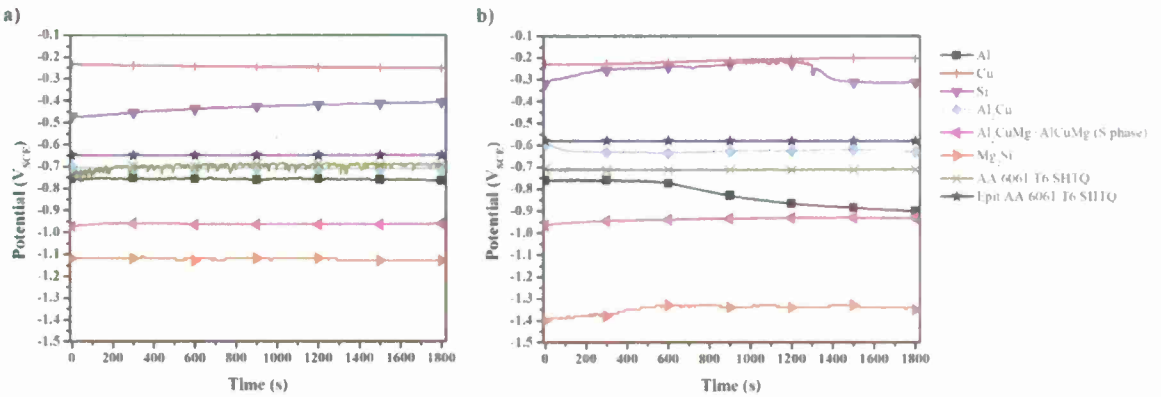

Figure 19. Open circuit potential versus time behavior for selected materials.(a) 30 minute OCP in aerated 0.6 M NaCl solution. (b) 30 minute OCP in 0.51 M NaCl + 12 mL 10.0 N HCl per liter, pH=1.2.

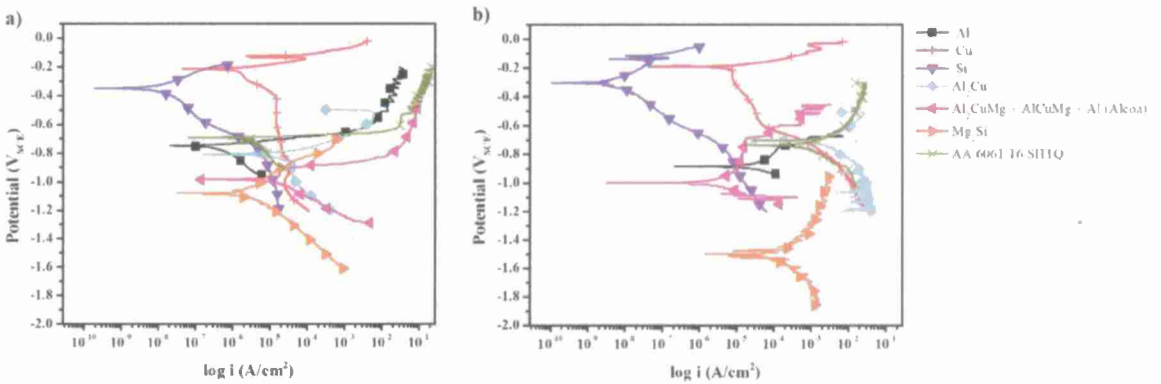

Figure 20. Anodic and cathodic polarization scans for selected materials.(a) E-log i behavior in aerated 0.6 M NaCl solution. (d) E-log i behavior in 0.51 M NaCl + 12 mL 10.0 N HCl per liter, pH=1.2. A 2 mm diameter aperture used on all tests, data uncorrected for ohmic resistance.

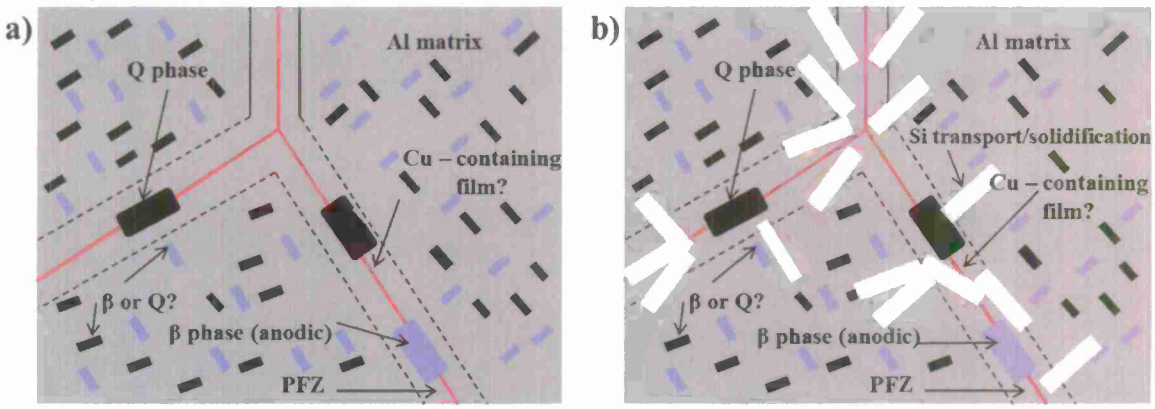

Figure 21. Schematic of a UNS A96061 microstructure at a grain boundary triple point in a wedge joint after brazing with UNS A94047 a) Region 4 and b) Regions 2-3. θ phase is not shown. Figures are modified and based on schematic presented by Svenningsen who reported a continuous Cu film [8].

6. Temper Optimization of AA 6061

The typical temper cycle for brazed AA 6061 is a T6 thermal cycle at 160 °C, followed by brazing, a room temperature aging to T4, and a final T6 hardening cycle. This brazing cycle (T6TCT6) results in precipitation of Mg-Si rich β and Q particle and also the Al_2Cu θ phase to grain boundaries within the braze region. These phases and the Si-precipitated microstructure lead to a galvanic couple to the α-Al matrix and result in preferential dissolution of the braze region and intergranular cracking.

This research explores an alternate braze thermal cycle (T4TCT6) in hopes of reducing the detrimental β, Q, and θ precipitates. In this thermal cycle, the initial T6 tempering step is removed. Instead, the T4 room temperature aging step precedes the brazing cycle which is then followed immediately by the final T6 strengthening temper step. In this approach, the braze cycles is not undertaken first.

The behavior of the T4TCT6 braze region was determined by an initial eletropolishing step, to highlight the presence of the different precipitates, and then after 8 hour immersion in acidified Cl^-. After electropolishing, significant Si precipitation is seen in near the braze region which decreases in density as distance from the braze region increases. After exposure, significant corrosion is seen within the braze region. The silicon rich braze zone show significant precipitate etching and IGC after immersion. A braze region after electropolishing and immersion test is shown in Figure 1. The T4TCT6 heat treatment cycle did not show beneficial reduction in precipitate formation or performance compared to the standard T6TCT6 heat treatment cycle.

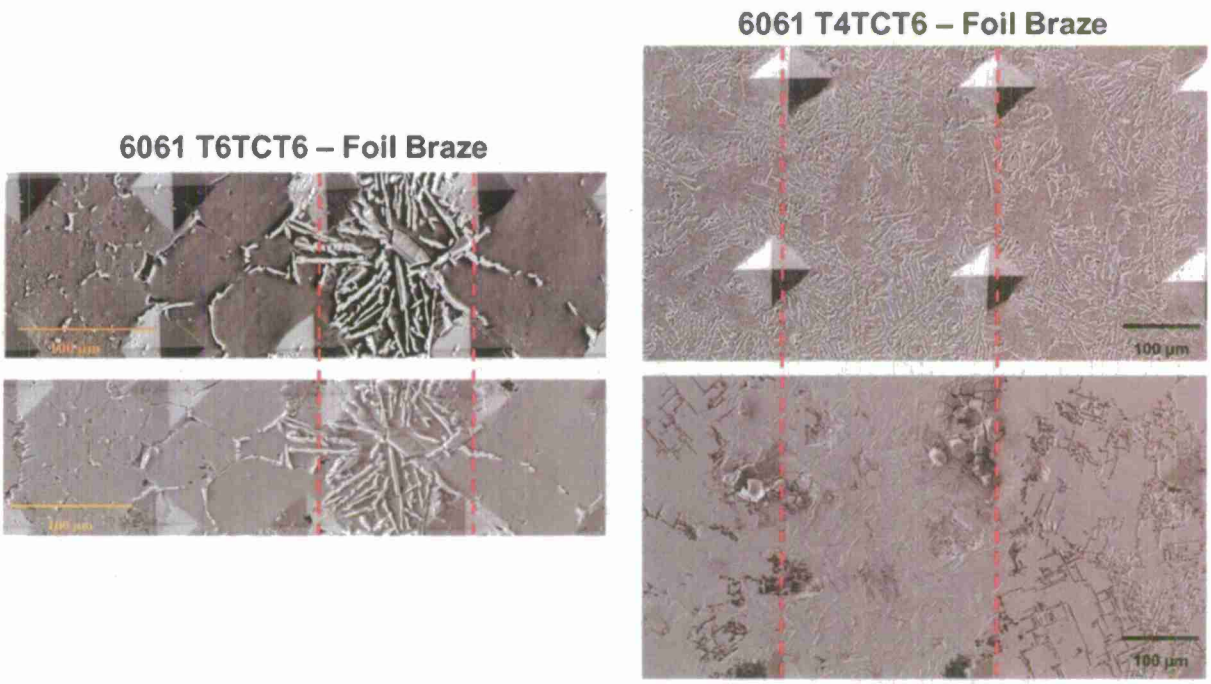

Figure 1. Comparison of brazed AA 6061 T6TCT6 **(left)** to brazed AA 6061 T4TCT6 **(right)** both foil AA 4047 filler material after electropolishing **(top)** and after 8 hour immersion in 0.51 M NaCl + 12 mL 10.0N HCl **(bottom)**. The braze region is between the dashed red lines on these micrographs.

7. Mitigation by Reduced Cu content by using 6063T52 + AA4047 Filler Foil (Low Cu Variants)

a. The strategy of reduced copper (Cu) is in an attempt to reduce detrimental θ, Q, S precipitates which all contain copper and may help promote corrosion and IGC.

Status: 6063T52 + AA4047 Filler Foil (Low Cu Variants) but the vendor (Coleman Micorwave) used past filler with Al-Si-Cu content which thwarted entirely the opportunity to study the Al-Si/Al-Si-Mg system with out Cu. Since this project has ended this investigation will not be performed.

8. TEM Studies of Precipitates at Grain Boundaries

Precipitation of second phase particles at grain boundaries during brazing cycle of AA6061 is detrimental to the corrosion resistance of the material. Intergranular corrosion in AA6061 after brazing cycle was observed using SEM after immersion tests. It is proposed that the corrosion morphology at the brazed region is dependent on the chemistry and distribution of the 2nd phase particles.

The objective of this study is to identify the 2nd phase particles precipitated at grain boundaries of AA6061 alloy after different brazing cycles. TEM and high resolution EDS techniques were used for this analysis. The specimens for TEM and EDS were mechanically ground with silicon carbide paper to approximately 80 μm thickness. The final thinning was conducted with ion-beam milling at 5 kV with the milling angle of 3 to 5 degree.

TEM images confirmed the existence of 2nd phase precipitate at grain boundaries of AA6061 T6 and AA6061 T6TCT6. These particles were elongated along the grain boundary with size of ca. 100 nm (Figures 2a, b and Figures 3a, b). EDS analysis identified that these particles were rich in Mg and Si (β phase) and Mg, Si, Cu and Al (Q phase) (Figures 2c, d and Figures 3c, d). Besides these 2 phases, the material also contained many constituent particles which were rich in Mg, Si, Cu, Fe and Cr. These constituent particles were mostly round in shape and were dispersed throughout the matrix.

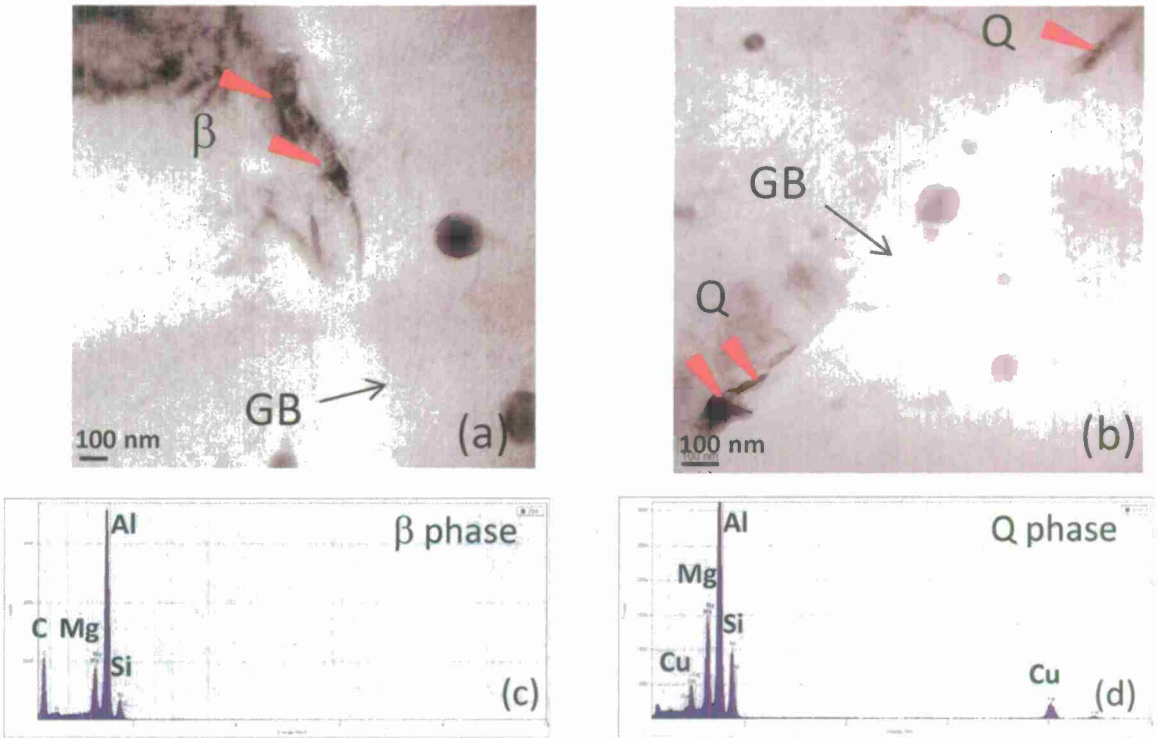

Figure 2. (a) and (b) BF-TEM images showing precipitate at grain boundary of AA6061 T6, (c) EDS of precipitate on Figure 2a, (d) EDS of precipitate on Figure 2b.

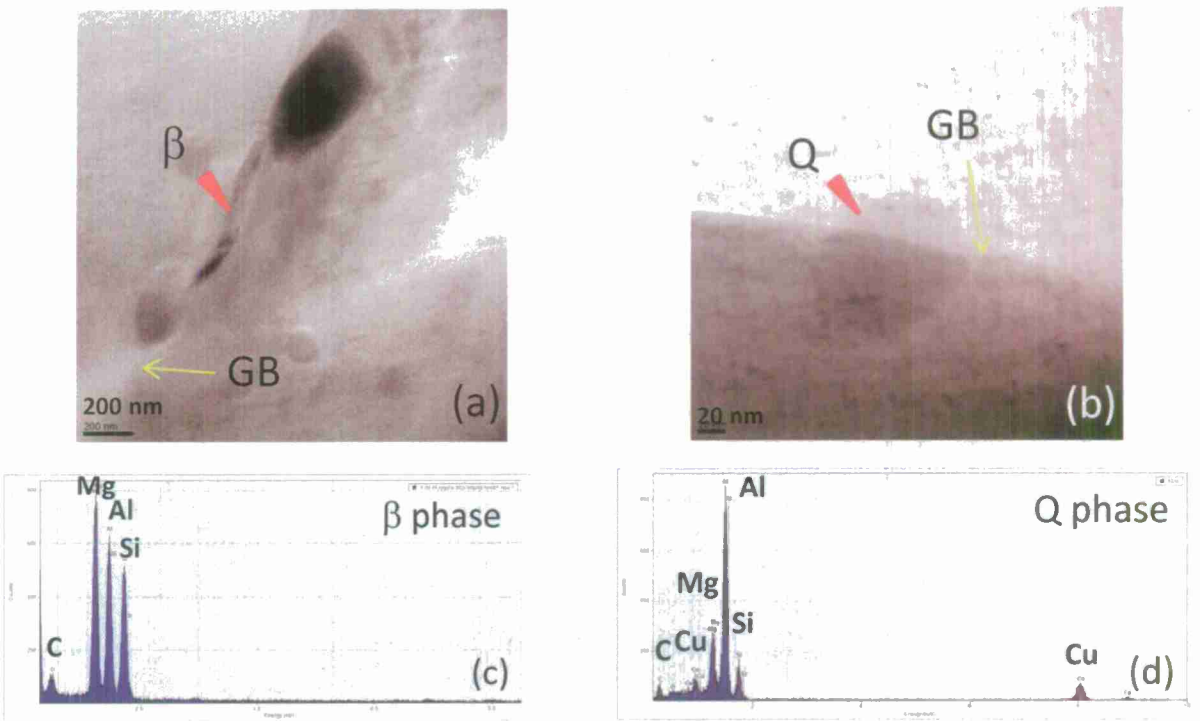

Figure 3. (a), (b) BF-TEM images showing precipitate at grain boundary of AA6061 T6TCT6, (c) EDS of precipitate on Figure 3a, (d) EDS of precipitate on Figure 3b.

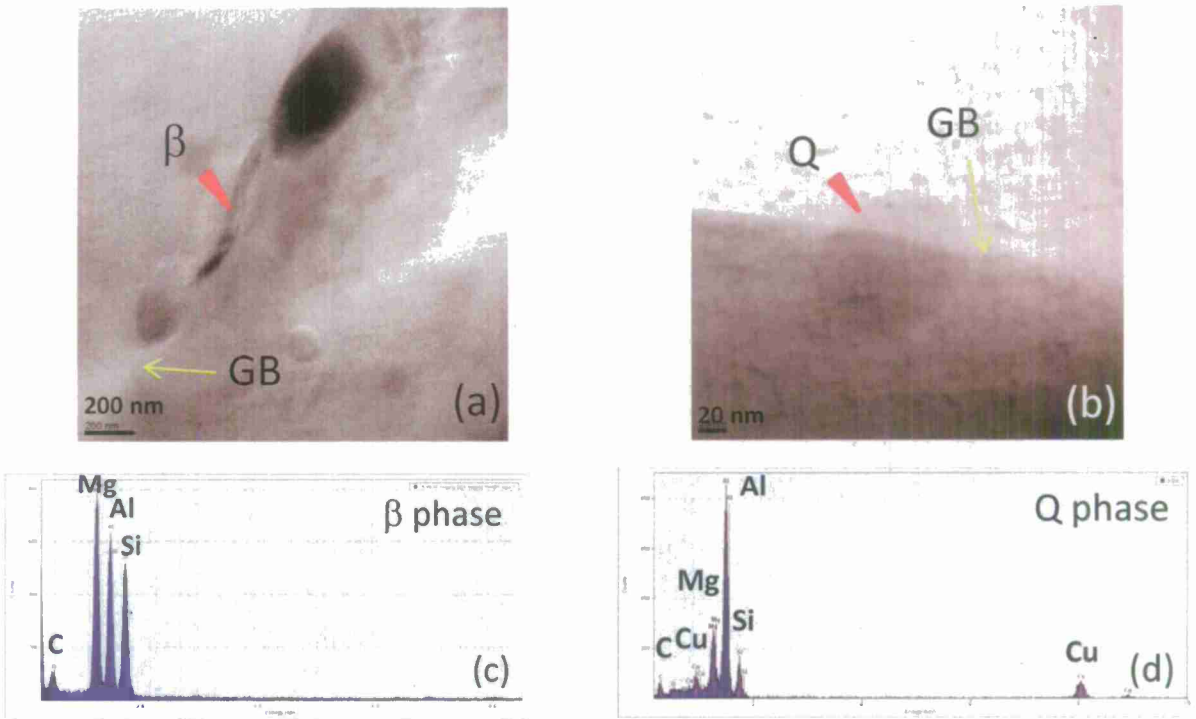

Figure 3. (a), (b) BF-TEM images showing precipitate at grain boundary of AA6061 T6TCT6, (c) EDS of precipitate on Figure 3a, (d) EDS of precipitate on Figure 3b.

9. Project Accomplishments

a. **Major awards/prizes/kudos received by PI :**

i. Fellow of the Society: American Society for Metals, National Association of Corrosion Engineers, Electrochemical Society
ii. NACE H.H. Uhlig Educator and A.B. Campbell Best Paper Awards (this grant)
iii. ECS H. Uhlig Award of the Corrosion Division
iv. UVA: Elected Charles Henderson Chair
v. NSF Presidential Young Investigator
vi. ASTM Frank La Que Award for Corrosion Science and Engineering
vii. T.P. Hoar Award for Best paper in Corrosion Science
viii. W.R. Whitney Award – NACE 2012
ix. Institute for Materials Research Chinese Academy of Science Lee Hsun Award
x. Co-author of over 200 archival papers, conference proceedings, books, book chapters in corrosion metallurgy area
xi. Chair of 2004 Gordon Research Conference
xii. Over 40 Invited Lectures in 10 Countries including 6 Gordon Conference Talks
xiii. National Service: National Academy of Engineering NMAB workshop and Study on Corrosion Education, DOE-OCRWM Panels and Workshop on Federal Repository at Yucca Mountain, Member Defense Science Board Task Force on Corrosion Control, DOE-BES Workshop on Research Needs, Gaps and Opportunities Concerning Corrosion at Yucca Mountain
xiv. Editorial boards: Technical Editor in Chief Corrosion Journal, associate editor Materials and Corrosion (Germany), past key reader Metallurgical and Materials Transactions
xv. Member: NACE, ECS, ASTM, NACE, ASM

b. **Approximate number of graduate students supported on this grant:**

i. 4 Graduate students have been supported and 3 undergraduates and 1 high school student
ii. Three of four have won student poster awards at an International Conference for Braze or Weld Sandwich work
iii. One A.B. Campbell Award for best paper for an author under 35 years of age
iv. Three women or minority
v. Two Post-doctoral Fellows
vi. One research scientist
vii. All GRAs - US citizen students with prominent positions in industry or government labs

c. **Major past accomplishments, (FY06-FY10) from ONR contract**

i. Defined New Corrosion Mechanisms in Brazed and Laser Welded SASS Sandwich Structures identifying role of melting point depressants other alloying elements and dissimilar metal crevice corrosion
ii. Defined Minimum braze clearance and post-weld heat treatments to maximize resistance to corrosion by these mechanisms
iii. Defined Governing Metallurgical, Environmental and Geometric Factors in Corrosion of Sandwich Structures that guide mitigation strategies
iv. Defined mitigation by alloy substitution, post-braze heat treatment, novel braze alloy design, control of weld or baraze parameters
v. Defined optimal weld parameters for good corrosion resistance and simultaneous weld penetration to achieve bonding
vi. Designed New Braze alloy based on combined metallurgical and corrosion design criteria using both computational and experimental methods

d. **Research Outcomes:**

i. Novel wedge shaped braze sample developed that enables corrosion testing at infinite number of braze gaps. This is a research first in the field of corrosion
ii. Braze alloy designed to enable harsh marine service with SASS sandwich structures
iii. Optimal weld conditions for bonding and corrosion resistance defined to enable harsh marine service with SASS sandwich structures
iv. Interaction with NSWC-CD, NAVSEA personnel on corrosion of sandwich materials
v. Patent disclosure on new braze alloy invention in preparation
vi. 4 Conference proceedings
vii. 3 archival journal research papers accepted; established leadership on corrosion of cellular metals
viii. Feedback to other research groups fabricating sandwich structures with corrosion resistance
ix. Three archival publications, 3 proceedings publications, 8 conference talks or posters

10. Publications – student co-author underlined

- J.R. Scully, W.L. Harris, "Opportunities and Challenges in Corrosion Education: Review of a National Research Council Assessment," The Electrochemical Society Interface, pp. 55-59. Spring (2012).
- K.M. Fleming, A. Zhu, J.R. Scully, "Corrosion of AA 6061 Brazed with an Al-Si-Cu Filler Paste: Effects of Si and Cuon Metallurgy and Corrosion," In preparation for CORROSION, (2012).
- K.M. Fleming, A. Zhu, J.R. Scully, "Corrosion of AA 6061 Brazed with an Al-Si Filler: Effects of Si on Metallurgy and Corrosion," CORROSION, Vol. 68, No. 12, pp. 1126-1145. (2012).
- K.M. Fleming, A. Zhu, J.R. Scully, "Corrosion of AA 6061 Brazed with an Al-Si Filler: Effects of Si on Metallurgy and Corrosion," DoD Corrosion Conference, Palm Springs, August (2011).
- J. James, J.M. Fitz-Gerald, J.R. Scully, "Localized Corrosion of a super-austenitic stainless steel (Fe-24Ni-20Cr-6.3Mo-0.22N) brazed with Ni-based braze (Ni-22Cr-6.3Si-3.8P): Effect of Braze Clearance on Corrosion Resistance," *Carrasian J.*, 65(8), pp. 511-526 (2009).
- S. Anastasio-Hebb, J. James, J. Fitz-gerald, G. Young, Jr., John R. Scully, "Corrosion of a super-austenitic stainless steel (Fe-24Ni-20Cr-6.3Mo-0.22N) brazed with Nicrobraz 31 (Ni-22Cr-6.3Si-3.8P): Electrochemical Corrosion Behavior of Isolated and Combined Materials," *Corrosion J.*, Vol. 65, No. 6, pg. 388-403, (2009).
- J.H. Macha, J.R. Scully, "Corrosion Properties of Laser-Welded Superaustenitic Stainless Steel Sandwich Structures, *Carrasian*, 65(7), pp 472-490 (2009).
- J.H. Macha, J.R. Scully, "Corrosion Properties of Laser-Welded Superaustenitic Stainless Steel Sandwich Structures, NACE Conference 2009, Atlanta GA, March, Paper 09196 (2009).
- J. James, J.M. Fitz-Gerald, J.R. Scully, *"Localized Corrasian af a super-austenitic stainless steel (Fe-24Ni-20Cr-6.3Ma-0.22N) brozed with Ni-based braze (Ni-22Cr-6.3Si-3.8P): Effect af Broze Clearance on Carrasion Resistonce,"* CORROSION/08, Paper No. 08256 (2008).
- S. Anastasio, J. James, J. Fitz-gerald, G. Young, Jr., John R. Scully, *"Carrasian af a super-austenitic stainless steel (Fe-24Ni-20Cr-6.3Ma-0.22N) brazed with Nicrabraze 31 (Ni-22Cr-6.3Si-3.8P): Electrochemicol Corrosion Behovior of Isoloted ond Combined Moteriols,"* CORROSION/08, paper No. 08257 (2008).
- J.R. Scully, **Environment Assisted Cracking**, in Francis LaQue Book on Corrosion in Seawater, (submitted) (2012).

11. Human Resource Development (9 year history)

Name	Rank at Graduation	Current Status
Mr. Joshua James	M.S. Degree MSE	DNV Columbus Ohio
Mr. John Macha	M.S. Degree MSE	Corpus Christi Army Helicoptor Depot
Ms. Katherine (Fleming) Holloran	M.S. Degree MSE	ExxonMobil Pipelines Co; Houston, TX
Ms. Sara (Anastasio) Hebb	M.S. Degree MSE	Solutia; Pensacola, FL
Dr. Florent Bocher	PDRA MSE	SWRI; San Antonio, TX
Dr. Derek Horton	Ph.D. degree MSE	NRL, Washington DC
Dr. Hung Ha	Research Scientist MSE	Univ. of Virgina
Dr. Ai-wu Zhu	Research Scientist MSE	Physics Teacher Governors School VA